NAVAL POSTGRADUATE SCHOOL
Monterey, California

DTIC
ELECTE
FEB 0 7 1992

THESIS

BOTTOM TRAPPED WAVES
AT TIDAL FREQUENCIES
OFF POINT SUR, CALIFORNIA

by

Stephen L. Sielbeck

September 1991

Co-Advisor   Steven R. Ramp
Co-Advisor   Leslie K. Rosenfeld

92-03119

Unclassified

security classification of this page

REPORT DOCUMENTATION PAGE

1a Report Security Classification Unclassified		1b Restrictive Markings		
2a Security Classification Authority		3 Distribution,Availability of Report		
2b Declassification Downgrading Schedule		Approved for public release; distribution is unlimited.		
4 Performing Organization Report Number(s)		5 Monitoring Organization Report Number(s)		
6a Name of Performing Organization Naval Postgraduate School	6b Office Symbol (if applicable) 3S	7a Name of Monitoring Organization Naval Postgraduate School		
6c Address (city, state, and ZIP code) Monterey, CA 93943-5000		7b Address (city, state, and ZIP code) Monterey, CA 93943-5000		
8a Name of Funding Sponsoring Organization	8b Office Symbol (if applicable)	9 Procurement Instrument Identification Number		
8c Address (city, state, and ZIP code)		10 Source of Funding Numbers		
		Program Element No	Project No	Task No	Work Unit Accession No

11 Title (include security classification) BOTTOM TRAPPED WAVES AT TIDAL FREQUENCIES OFF POINT SUR, CALIFORNIA

12 Personal Author(s) Stephen L. Sielbeck

13a Type of Report Master's Thesis	13b Time Covered From To	14 Date of Report (year, month, day) September 1991	15 Page Count 71

16 Supplementary Notation The views expressed in this thesis are those of the author and do not reflect the official policy or position of the Department of Defense or the U.S. Government.

17 Cosati Codes			18 Subject Terms (continue on reverse if necessary and identify by block number)
Field	Group	Subgroup	bottom trapped waves, diurnal, semidiurnal, continental slope currents, tidal currents

19 Abstract (continue on reverse if necessary and identify by block number)

Current meter data were collected from moorings on the 800 and 1800 m isobaths on the continental slope off Point Sur, California at 100, 350, and 500 m depth and at 1000 m depth on the 1800 m isobath. Complex demodulation and spectral techniques were used to study the distribution of tidal energy at the diurnal and semidiurnal frequencies, and to study the size, rotation and orientation of the tidal current ellipses. At mooring P2 (800 m) the observed diurnal energy increased with depth for each of the 17 months of data analyzed, and the semidiurnal energy likewise increased with depth for 14 of the 17 months. The observations were studied using the theory of bottom trapped waves in a rotating stratified fluid (Rhines, 1970). Bottom trapping is expected at the diurnal and semidiurnal frequencies whenever the critical trapping frequency $\omega_c = N \sin\alpha \sin\phi$ exceeds 1/24 and 1/12 hours^{-1} respectively, where N = the Brunt-Väisälä frequency, α the bottom slope, and ϕ is a measure of the angle the wavenumber vector makes with the gradient of topography. Theoretical energy decay curves matched the observed energy levels at P2 very well, indicating that the enhancement of energy with depth was likely due to the presence of bottom trapped waves. No bottom trapping was observed at P3 (1800 m) because the deepest current meters were positioned too far above the sea floor to detect bottom trapped energy, and because the density gradients near the sea floor were weaker than at site P2 and kept ω_c below the tidal frequencies.

20 Distribution/Availability of Abstract ☒ unclassified/unlimited ☐ same as report ☐ DTIC users	21 Abstract Security Classification Unclassified	
22a Name of Responsible Individual Steven R. Ramp	22b Telephone (include Area code) (408) 646-3162	22c Office Symbol OC/Ra

DD FORM 1473,84 MAR

83 APR edition may be used until exhausted
All other editions are obsolete

security classification of this page

Unclassified

Approved for public release; distribution is unlimited.

Bottom Trapped Waves
at Tidal Frequencies
Off Point Sur, California

by

Stephen L. Sielbeck
Lieutenant Commander, United States Coast Guard
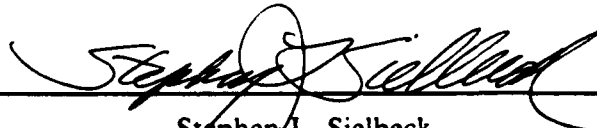B.S., United States Coast Guard Academy, 1979

Submitted in partial fulfillment of the
requirements for the degree of

MASTER OF SCIENCE IN PHYSICAL OCEANOGRAPHY

from the

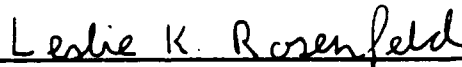NAVAL POSTGRADUATE SCHOOL
September 1991
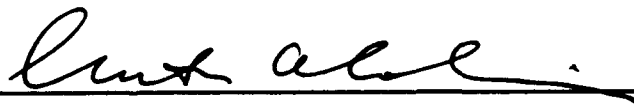
Author: _____

Stephen L. Sielbeck

Approved by: _____

Steven R. Ramp, Co-Advisor

_____

Leslie K. Rosenfeld, Co-Advisor

_____

Curtis A. Collins, Chairman,
Department of Oceanography

ii

ABSTRACT

Current meter data were collected from moorings on the 800 and 1800 m isobaths on the continental slope off Point Sur, California at 100, 350, and 500 m depth and at 1000 m depth on the 1800 m isobath. Complex demodulation and spectral techniques were used to study the distribution of tidal energy at the diurnal and semidiurnal frequencies, and to study the size, rotation and orientation of the tidal current ellipses. At mooring P2 (800 m) the observed diurnal energy increased with depth for each of the 17 months of data analyzed, and the semidiurnal energy likewise increased with depth for 14 of the 17 months. The observations were studied using the theory of bottom trapped waves in a rotating stratified fluid (Rhines, 1970). Bottom trapping is expected at the diurnal and semidiurnal frequencies whenever the critical trapping frequency $\omega_c = N\sin\alpha\sin\phi$ exceeds 1/24 and 1/12 hours^{-1} respectively, where N = the Brunt-Väisälä frequency, α the bottom slope, and ϕ is a measure of the angle the wavenumber vector makes with the gradient of topography. Theoretical energy decay curves matched the observed energy levels at P2 very well, indicating that the enhancement of energy with depth was likely due to the presence of bottom trapped waves. No bottom trapping was observed at P3 (1800 m) because the deepest current meters were positioned too far above the sea floor to detect bottom trapped energy, and because the density gradients near the sea floor were weaker than at site P2 and kept ω_c below the tidal frequencies.

iii

TABLE OF CONTENTS

LIST OF TABLES

vi

LIST OF FIGURES

I. INTRODUCTION

A. BACKGROUND

The Naval Postgraduate School maintained an array of subsurface current meter moorings off Point Sur, California from 1989 to 1990. The moorings were positioned on the continental slope and collected data used in the study of the California Current System (Figure 1). The initial spectral analysis of data from mooring P2 indicated that the kinetic energy at diurnal tidal frequencies increased with depth (Figure 2). This was an unusual phenomena because vertical energy structures at tidal frequencies are usually associated with the baroclinic modes of free internal waves. At the latitude of Point Sur (36° 20′ N) the inertial frequency is approximately 1.1 cpd and free internal waves cannot exist at diurnal (subinertial) frequencies. Baroclinic waves can exist at subinertial frequencies only if the waves are trapped along a wall or slope.

The tides off most of the California coast are a mixture of diurnal and semidiurnal components. The principal lunar constituent, M_2, is the strongest tidal element followed by the K_1, O_1, and S_2 constituents. Barotropic diurnal and semidiurnal tides both propagate northward along the coast. The semidiurnal tide is a combination of Kelvin, Poincare and forced waves. The barotropic semidiurnal tidal current ellipses, representing horizontal current amplitudes and directions, are generally oriented parallel to the coastline (*Munk et al.*, 1970). The barotropic diurnal tide is a combined Kelvin and shelf wave with current ellipses which can be either parallel or perpendicular to topography (*Noble et al.*, 1987). Several studies of California tides have found the primary direction of rotation for diurnal and semidiurnal current ellipses to be counterclockwise.

Baroclinic tides are generated when semidiurnal surface tides force isopycnal surfaces over topographic features, such as the continental shelf break (*Wunsh*, 1975).

1
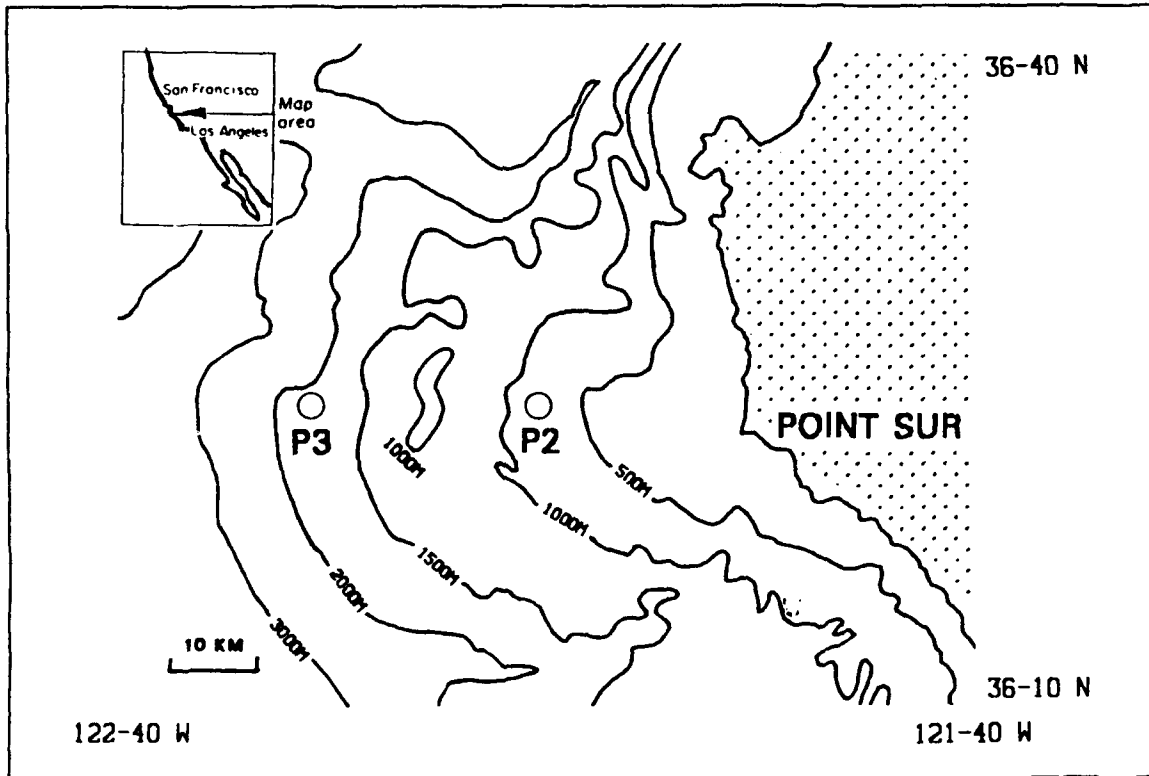
Figure 1.   Point Sur Moorings P2 and P3:   The location of Point Sur on the California coast is shown in the inset.

While the barotropic semidiurnal tide is usually aligned with topography, internal tides often become the dominant cross-slope current component along the California coast (*Noble et al.*, 1987).

Variations in the vertical distribution of tidal energy have been observed at semidiurnal frequencies. During the Coastal Ocean Dynamics Experiment (CODE), the baroclinic semidiurnal internal tide was larger than the barotropic tide. Changes in semidiurnal kinetic energy at different depths were linked to surface winds and changing stratification (*Rosenfeld*, 1990). The semidiurnal internal tides observed in CODE had some bottom energy intensification which was attributed to the horizontal velocity structure of the first dynamic mode.
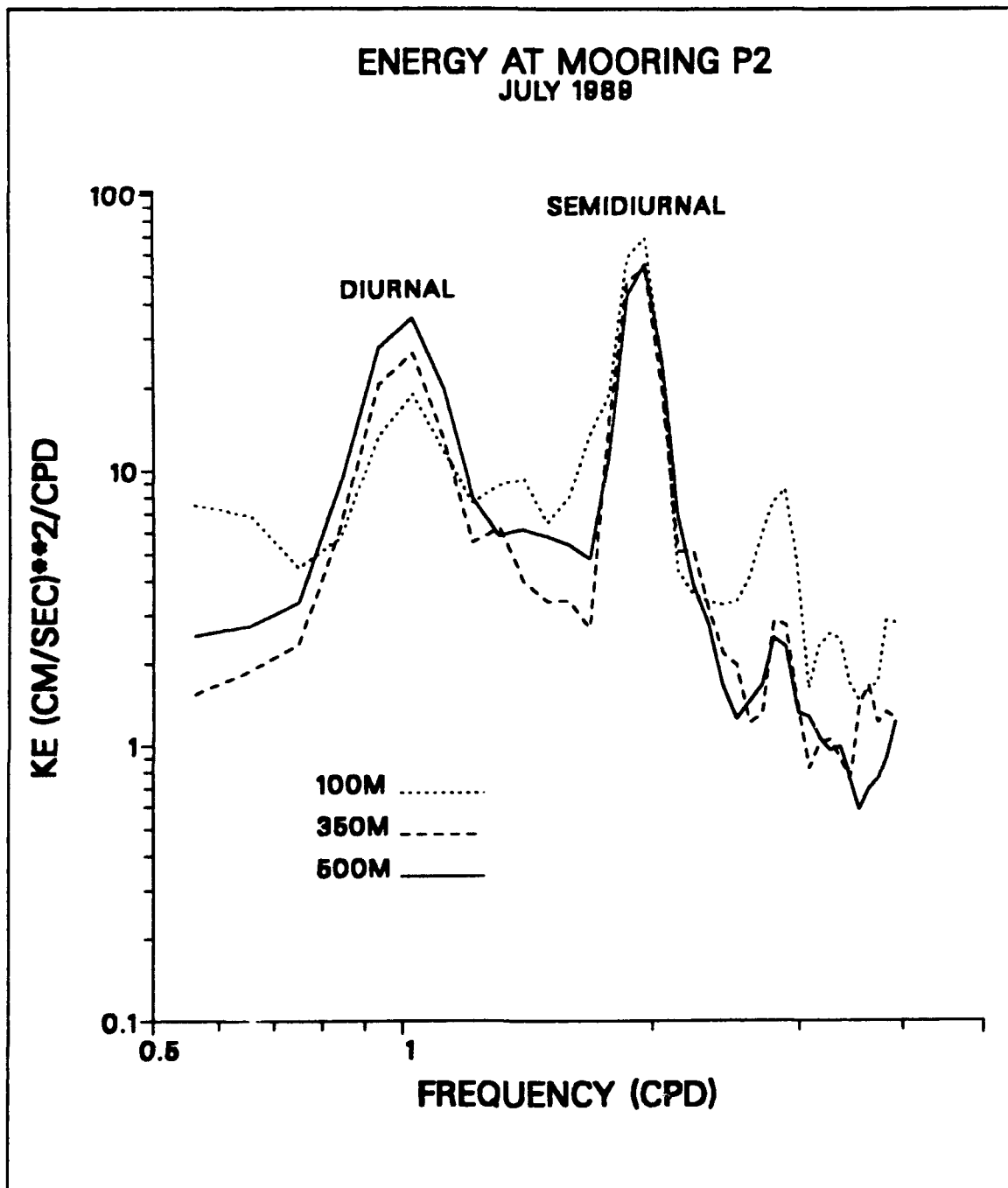
Figure 2. Spectral Analysis of Energy at Mooring P2 During July 1989: The curves represent energy at 100 m, 350 m and 500m.

There are few published studies which discuss similar bottom intensification of subinertial currents. Bottom trapped topographic Rossby waves were observed by

3

Thompson and Luyten (1976) and were discussed using bottom trapped wave theory developed by Rhines (1970). These were low frequency waves, however similar theory was applied to bottom trapped waves at tidal frequencies and used to study the tidal currents and vertical energy distribution off Point Sur.

B. BOTTOM TRAPPED WAVES IN A ROTATING STRATIFIED FLUID

This discussion follows the development presented by Rhines (1970) for bottom trapped waves in a uniformly stratified, rotating fluid bounded by a single plane wall inclined everywhere at angle α to the horizontal. A right handed orthonormal coordinate system is oriented on the slope such that the x_1 and x_2 axis are rotated at an angle ϕ from the alongslope and upslope directions respectively and x_3 is perpendicular to the bottom slope (Figure 3). The corresponding velocities along x_1, x_2 and x_3 are designated as u_1 , u_2 and u_3 .

The governing equations are the linearized, non-diffusive Boussinesq equations used in the form:

$$\frac{\partial \mathbf{u}}{\partial t} + 2\Omega \mathbf{u} = -\frac{\nabla p}{\rho_0} - g\rho' \hat{\jmath} \tag{1}$$

$$\frac{\partial \rho'}{\partial t} = \frac{N^2}{g} \mathbf{u}\hat{\jmath} \tag{2}$$

where p = pressure, Ω = angular rotation of the earth, g = gravitational acceleration, $\hat{\jmath}$ = a vertical unit vector, $2\Omega = f\hat{\jmath} = f(\sin\alpha\sin\phi, \sin\alpha\cos\phi, \cos\alpha)$, $f =$ Coriolis parameter, the Brunt-Väisälä frequency squared $= N^2 = \frac{-g}{\rho_0}\frac{\partial p_1}{\partial z}$, and a perturbation density is used such that $\rho = \rho_0 + \rho(z) + \rho'(x, y, z, t)$.

Inviscid boundary conditions are chosen so that $u_3 = 0$ at $x_3 = 0$. If $u_3 = 0$ everywhere in the water column the motion is nondivergent in planes perpendicular to the x_3 axis and the continuity equation $\frac{\partial u_1}{\partial x_1} + \frac{\partial u_2}{\partial x_2} = 0$ applies. The wave propagates in the

4
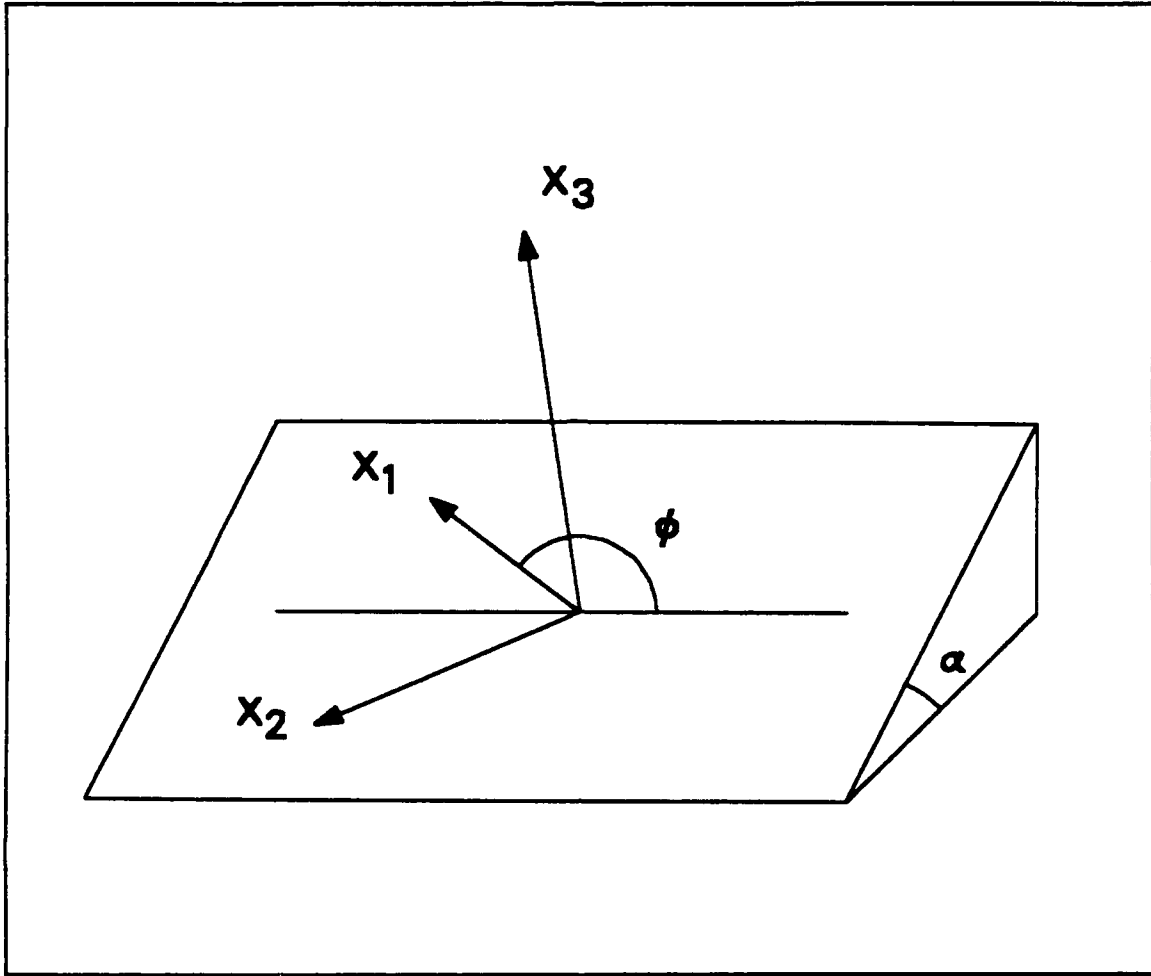
Figure 3. Coordinates for Bottom Trapped Waves on a Sloping Bottom: The elevation from the horizontal is given by α.

x_2 direction with $\dfrac{\partial u_1}{\partial x_1} = 0$. To balance the continuity equation $\dfrac{\partial u_2}{\partial x_2}$ must also equal

zero. When $u_2 \neq 0$ and $\dfrac{\partial}{\partial x_2} = 0$, free internal waves can exist. If $u_2 = 0$ and $\dfrac{\partial}{\partial x_2} \neq 0$

waves are trapped against the wall (bottom) in a plane parallel to the boundary surface

with particle motion limited to the x_1 direction.

Substituting u_1, $u_2 = u_3 = 0$, and the appropriate form of 2Ω into Equations (1) and

(2) leads to a set of three equations where for the x_1 direction, Equation (1) becomes

$$\frac{\partial u_1}{\partial t} = -g\rho'(\sin\alpha\sin\phi) \tag{3}$$

In the x_2 direction, Equation (1) becomes

$$fu_1(\cos\alpha) = -\frac{1}{\rho_0}\left(\frac{\partial p}{\partial x_1} + \frac{\partial p}{\partial x_2} + \frac{\partial p}{\partial x_3}\right) - g\rho'\hat{j}$$

$$fu_1(\cos\alpha) = -\frac{1}{\rho_0}\frac{\partial p}{\partial x_2} - g\rho'(\sin\alpha\cos\phi) \tag{4}$$

For the x_3 direction, the result is

$$-fu_1(\sin\alpha\cos\phi) = -\frac{1}{\rho_0}\frac{\partial p}{\partial x_3} - g\rho'(\cos\alpha) \tag{5}$$

The rate of change of the density perturbation, equation (2), similarly reduces to

$$\frac{\partial\rho'}{\partial t} = \frac{N'^2}{g}u_1(\sin\alpha\sin\phi). \tag{6}$$

The combination of equations (3) and (6) results in an expression for the frequency σ where:

$$\left(\frac{\partial\rho'}{\partial t}\right)\left(\frac{\partial u_1}{\partial t}\right) = (N^2 u_1\rho')(\sin\alpha\sin\phi)^2$$

$$\frac{\partial^2}{\partial t^2}(\rho'u_1) = N^2 u_1\rho'(\sin\alpha\sin\phi)^2$$

$$\sigma^2 = N^2(\sin\alpha\sin\phi)^2$$

$$\sigma = \pm N\sin\alpha\sin\phi \tag{7}$$

6

Substituting (7) into (6), ρ' can be determined as

$$\rho' = \frac{N}{g} u_1 \tag{8}$$

Solutions to the wave equations are found using the form

$$p = p_0 e^{(-\kappa + lk_3)x_3 + l(k_2 x_2 - \sigma t)} \tag{9}$$

where κ and k_3 are real. κ is defined as a trapping coefficient with units of wavenumber. The alongslope or horizontal (k_2) and vertical (k_3) wavenumbers in this solution lead to spatial dependence in the x_2 and x_3 directions. Using equations (8) and (9) in (4) and (5), the spatial dependence of the wave is:

$$\frac{\kappa}{k_2} = \frac{S[1 - \sin^2\alpha \sin^2\phi]}{\cos^2\alpha + S^2 \sin^2\alpha \cos^2\phi} \; \mathrm{sgn}(\sin\alpha \sin\phi) \tag{10}$$

$$\frac{k_3}{k_2} = \frac{1}{2} \frac{(1 - S^2)\sin 2\alpha \cos\phi}{\cos^2\alpha + S^2 \sin^2\alpha \cos^2\phi} \tag{11}$$

where $S = \frac{N}{f}$. When the trapping coefficient κ is positive the wave motion is exponential and trapped near the bottom. From equation (9), wave motion decreases due to the effect of trapping by

$$e^{-\kappa x_3} \tag{12}$$

The magnitude of trapping is dependent upon α and ϕ. When particle motion is directly up the slope ($\phi = 90°$) trapping is maximized. When particle motion is along the isobaths ($\phi = 0°$), no trapping occurs.

Rhines discusses four different geometries where trapping occurs: (1) $\alpha \sim 1$ for steep slopes, (2) $\alpha \sim S^{-1}$ for more gradual slopes such as those on the continental slope, (3)

7

$\alpha \ll S^{-1}$ for very gradual slopes such as those on the continental rise, and (4) $\frac{\pi}{2} - \alpha \ll S \cos \phi$ for near vertical slopes. Consider the case appropriate for the continental slope off the California coast where $\alpha \sim S^{-1}$ and $\sin \phi \sim O(1)$. Evaluating equation (7) using these relationships leads to the following:

$$\sigma = \pm N \sin \alpha \sin \phi \sim N \sin(S^{-1}) \sin \phi \sim N \frac{f}{N}$$

$$\sigma \sim f \qquad (13)$$

$\frac{\kappa}{k_2}$ can be expressed as:

$$\frac{\kappa}{k_2} = \frac{S[1 - \sin^2 S^{-1} \sin^2 \phi]}{\cos^2 S^{-1} + S^2 \sin^2 S^{-1} \cos^2 \phi} = S \qquad (14)$$

The ratio of $\frac{k_3}{k_2}$ reduces to

$$\frac{k_3}{k_2} = \frac{S[1 - \sin^2(S^{-1}) \sin^2 \phi]}{\cos^2(S^{-1}) + S^2 \sin^2(S^{-1}) \cos^2 \phi} = S \qquad (15)$$

The relationships now established with $\alpha \sim S^{-1}$ are $\sigma \sim f$, $\frac{\kappa}{k_2} \sim S$, and $\frac{k_3}{k_2} \sim S$. Parallel to the slope Coriolis is balanced by buoyancy as shown in equation (15). Coriolis traps waves against the wall (bottom) but the frequency of these trapped waves, determined by equation (7), is not dependent on f. Bottom trapped internal waves are similar to internal Kelvin waves because they are not bound by a lower frequency limit of f and trapped waves can exist and propagate at subinertial frequencies. The high frequency limit of bottom trapped waves is σ and is a function of α and N. Maximum trapping will always occur when $\phi = 90°$ and the particle motion is directly up the slope.

8

The exponential decay of trapped waves away from the bottom is determined by trapping coefficients. To determine κ, bottom trapped waves were assumed to have a dispersion relationship similar to baroclinic Kelvin waves (*Rhines*, 1970) where

$$\omega_n^2 = \frac{N^2 k^2}{k^2 + \left(\frac{n\pi}{H}\right)^2} \qquad n = 1, 2, 3 \ldots$$

with ω the frequency of a wave, k a horizontal wave number, n the mode number and H the water depth. The use of this dispersion relationship represents an approximation because baroclinic Kelvin waves assume a flat ocean bottom. The horizontal wave number can then determined using

$$k^2 = \omega_n^2 \frac{\left(\frac{n\pi}{H}\right)^2}{(N^2 - \omega_n^2)}$$

When $\phi = 90°$ waves are propagating along the slope in the x_2 direction and particle motion is up and down the slope in the x_1 direction. Trapping coefficients are defined as $\kappa = k_2 S$ from equation (14) and can be calculated using

$$\kappa = \frac{N}{f} \sqrt{\frac{\omega_n^2 \left(\frac{n\pi}{H}\right)^2}{(N^2 - \omega_n^2)}} \qquad (16)$$

Waves are trapped closer to the sea floor and decay more rapidly away from the bottom when κ increases. Trapping coefficients increase when (1) the buoyancy frequency N increases, (2) depth H decreases, (3) higher frequencies ω are considered (in the tidal range of 1.0 to 2.0 cpd), (4) f decreases (lower latitudes) and (5) for higher modes n. Trapping is weakest and waves decay more gradually away from the bottom in the first baroclinic mode. No trapping occurs for the barotropic case when $n = 0$.

9

II. DATA COLLECTION

A. CURRENT METER DATA

Current data were collected at two sites off Point Sur, California (Table 1) located over the continental slope ($\bar{\alpha} = .06$).

Table 1.   POINT SUR MOORING LOCATIONS

Mooring	Position	Depth
P2	36-20.0 N 122-10.2 W	800 m
P3	36-20.0 N 122-27.6 W	1800 m

Mooring P2, on the 800 m isobath, was equipped with three Aanderaa vector averaging current meters (RCM8) at depths of 100 m, 350 m and 500 m. Mooring P3 was situated 52 km offshore in 1800 m with four Aanderaa current meters at depths of 100 m, 350 m, 500 m and 1000 m (Figure 4).

Vector averaged current velocities, current directions, temperature, conductivity and pressure measurements were recorded every 30 minutes in a solid state Data Storage Unit (DSU). The DSU had a storage capacity of 65530 10-bit words and could record seven months of data with the sampling interval used. Sampling times were regulated by an internal quartz clock with an accuracy of ± 2 seconds per day. Several deployments were necessitated by the seven month data storage limit (Figure 5). P2 was recovered and redeployed in May, August and December 1989 and May 1990. The three current meters used on P2 provided nearly continuous data from May 1989 through October 1990. Mooring P3 was deployed in December 1989 and again in May 1990. Good data was obtained at four levels from December 1989 to April 1990. After April, the data from the current meters at 500 m and 1000 m was limited by instrument failures.

10
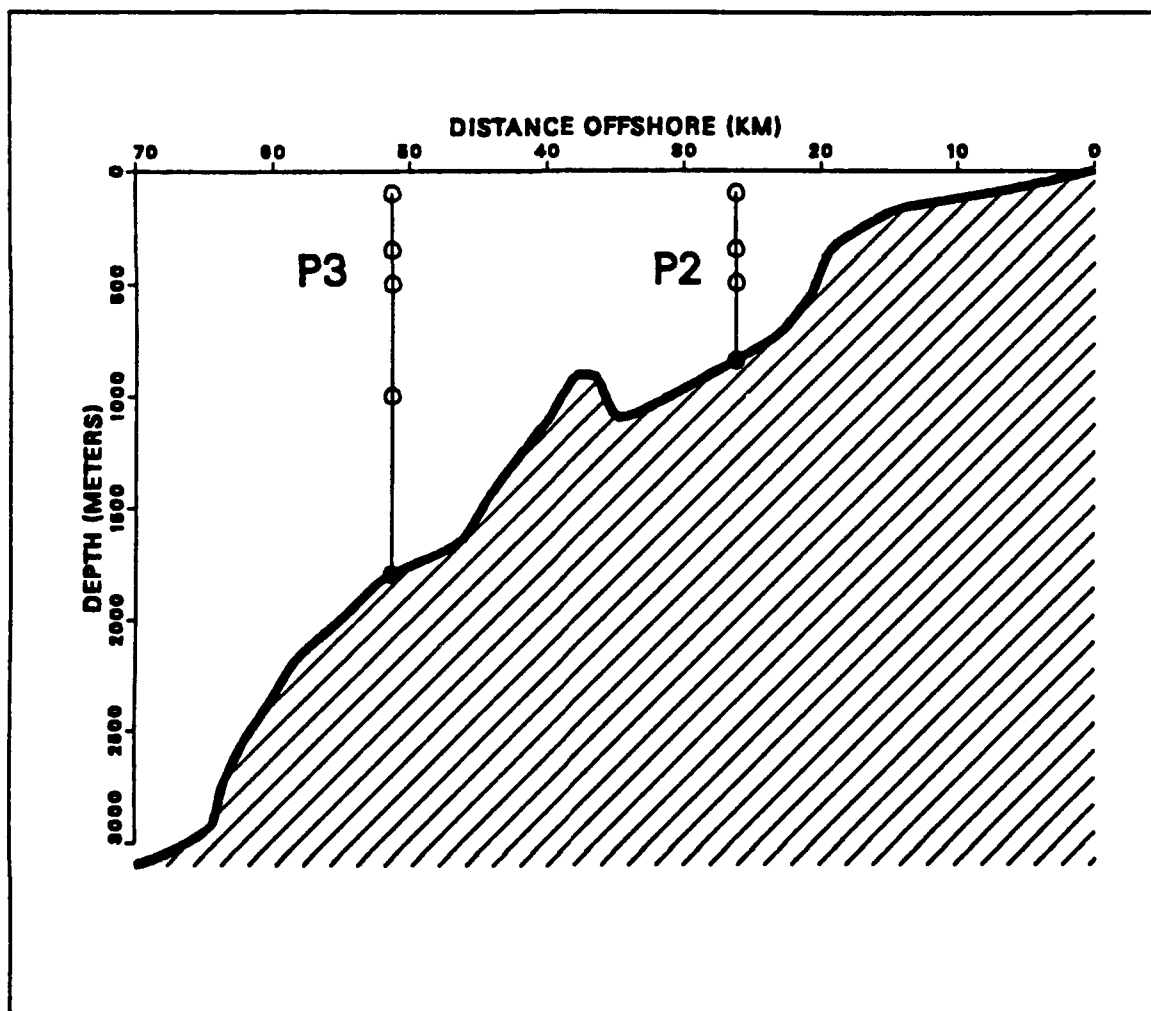
Figure 4. Current Meter Configuration at Moorings P2 and P3

Velocities were measured using a shrouded paddlewheel at the top of the recording

unit. The paddlewheel was magnetically coupled to an electronic counter and velocities,

in units of cm sec⁻¹, were determined by the number of revolutions the paddlewheel

made during each sampling interval. The sensor had a range of 2 - 250 cm sec⁻¹ with

an accuracy of ± 1.0 cm sec⁻¹ or ± 2 percent of the current velocity. The paddlewheel

stalled at velocities below a threshold of 2.0 cm sec⁻¹ (*Aanderaa*, 1990). The cosine re-

sponse was acceptable within ± 27° from the vertical. Both the pressure sensors and the

11
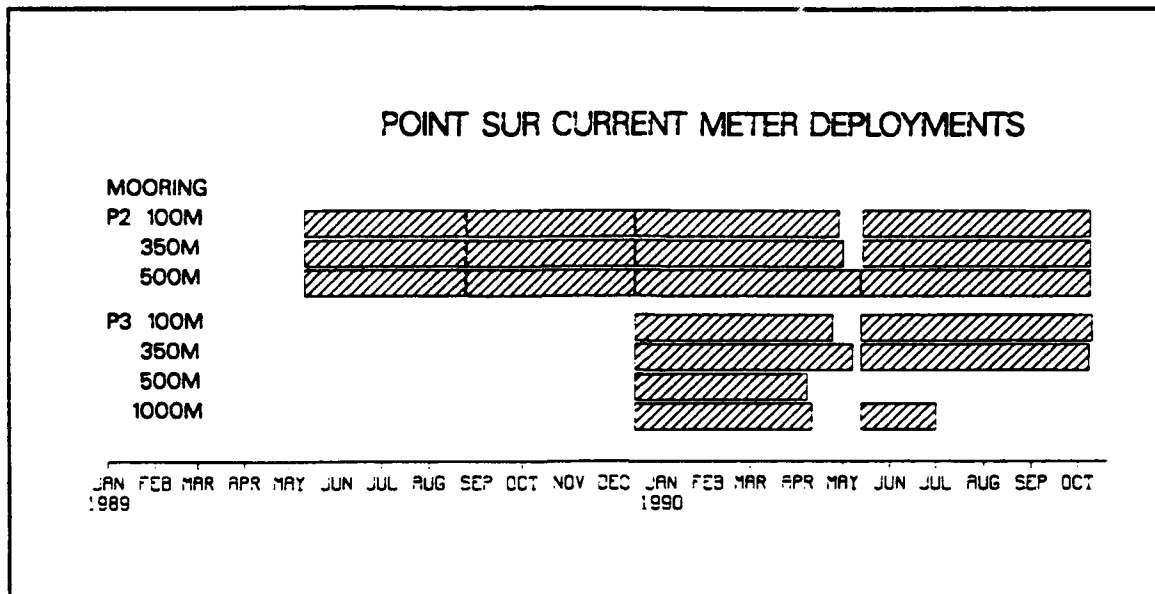
Figure 5. **Current Meter Deployments at Moorings P2 and P3:** The shaded bars indicate the intervals where good data was obtained at each depth.

mooring dynamics program in use at NPS indicated a maximum mooring tilt of 11.7° which was well within acceptable limits.

The current meters were oriented into the current by a large vane with an area of 2425 cm². The direction sensor was a magnetic compass with a potentiometer located at the bottom of the recording unit. The compass was oil damped and required 3 to 5 seconds to resolve changes of 90° or more. The resolution of the compass was 0.35° with an accuracy of ± 5° for velocities 5 - 100 cm sec⁻¹ and ± 7.5 degrees for velocities of 2.5 - 5.0 cm sec⁻¹ and 100 - 200 cm sec⁻¹. The compass could function properly with a maximum tilt angle of 12° from the vertical. Prior to each deployment the combined magnetic deviation and variation of each unit was determined on a surveyed test bench at the Naval Postgraduate School and the necessary corrections were applied via postprocessing software.

B. HYDROGRAPHIC DATA

While the current meters were deployed, several oceanographic research cruises were conducted in the region by the Naval Postgraduate School. These voyages consisted of California Undercurrent (CU) and Student Cruises (ST) which collected CTD data at intervals of approximately 10 km along the Point Sur Transect (POST). Data were collected near the moorings from the surface to within 50 - 150 m of the bottom using a Neil Brown Instruments System (NBIS) Mark IIIB CTD and are described in detail in Tisch (1990). Using the data from the cruises (Table 2), the various characteristics of the waters off Point Sur were examined. Although the station locations and spacing varied slightly with each cruise, the CTD data necessary for interpretation of the current meter results were comparable.

Table 2. HYDROGRAPHIC CRUISES OCCURRING DURING CURRENT METER DEPLOYMENTS

Cruise Designation	Date of CTD Casts
STMAY89	5/5/89
CUJUL89	7/29/89
CUSEP89	9/26/89
STNOV89	11/2/89
CUJAN90	1/18/90
CUMAR90	3/2/90
STMAY90	5/2/90
CUJUN90	6/27/90

III. METHODS OF ANALYSIS

A. SMOOTHING AND FILTERING

Upon recovery, the current meter DSU's were downloaded into a computer. The raw data files were converted standard scientific units using the sensor calibration equations and stored as formatted ASCII files. All data records were plotted to facilitate visual inspections. Velocity records were truncated where instrument failures or malfunctions were evident. Spurious values, such as an occasional outlier, were edited or deleted manually.

All data were band pass filtered prior to further analysis to isolate the frequencies of interest. The filtering and interpolation methods used were originally developed by Oregon State University (*Denbo et al.*, 1984). Postprocessed records, containing data at 30 minute intervals, were first low passed filtered (LP) using a Cosine-Lanczos filter. Such a filter minimizes unwanted ringing or oscillations caused by the Gibbs phenomena while still providing a sharp roll off at the desired cutoff frequency. A centered 25 point segment of the records was used to produce each LP filtered data point. The LP filter had a half power period of 2.9 hours (or a frequency of 8.4 cpd). The filter allowed any signal with a period exceeding 3.6 hours to pass through unattenuated. Signals with a period of less than 2.0 hours were removed entirely. After the LP filtering, records were interpolated to transform 30 minute data records to 60 minute intervals with each data point falling on an even hour. The interpolation routine utilized Lagrangian polynomials to interpolate any unevenly spaced data points (due to missing individual data points or outliers) to specific time intervals (*Gerald and Wheatly*, 1989). After interpolation, the data was again low passed filtered (LLP). The second Cosine-Lanczos filter had a half power period of 46.59 hours (or a frequency of 0.515 cpd) and used a

centered 121 point segment to produce one filtered data point. This filter was designed to remove diurnal and shorter period tidal energy and any inertial frequency energy present in the signal. The LLP records were subtracted from the LP records to produce the band passed form used in the tidal analysis. A sample from 100 m at P2 (Figure 6) shows the results of the filtering procedures.

B. TIDAL COMPONENTS

1. Harmonic Analysis

To understand the nature of the tidal currents, an analysis of the various tidal components was desired. Traditional harmonic tidal analysis, or the technique of linear combinations, requires a complete set of observations over a standard length period. Tidal heights or motions can be expressed as a sum of harmonic terms, each determined by a known, fixed frequency. A single estimate of the amplitude and phase are then extracted through the analysis of observations. Observational periods are normally multiples of synodic periods involving the most important tidal constituents. The preferred record length for a complete tidal analysis is 369 days. This allows extraction of the amplitude and phase of at least 64 of the largest tidal constituents (*Dronkers, 1964*). An adequate description of the major constituents can be accomplished using a much shorter observation of 29 days. A 14 day time series is adequate to provide the resolution of the principal diurnal constituents, K_1 and O_1, and a 15 day time series will resolve the principal semidiurnal constituents M_2 and S_2. Some of the longest tidal constituents require a full 19 year record for accurate resolution (*Schureman, 1958*).

The current records collected off Point Sur vary in length and are not ideally suited for the method of linear combinations. The traditional method could provide only a few independent estimates of the tidal constituents for each month of recorded current observations. Complex demodulation, a least squares analysis technique, was used instead to accomplish the harmonic analysis. The primary advantage realized with this

15

Figure 6. **Current Meter Record Filtering:** Time series from mooring P2 at 100 m showing velocities in cm sec⁻¹ with LP filtering, LLP filtering and the band passed residual for the *u* (top three panels) and *v* (lower three panels) components.

16

method is that records of any length can be analyzed. Complex demodulation utilizes a set of normal equations which are solved for unknown amplitudes and phase corresponding to n frequency constituents. The number of unknowns solved for in the set of equations is $2n + 1$. The number of equations used in each set is determined by the number of observations, m, utilized for each estimate and the solutions are determined using matrix algebra. Schematically, this process an be represented as

[observed velocities] = [known tidal constants][unknown empirical constants]

The least squares method minimizes the difference between an observed current velocity and the sum of the solutions corresponding to that observation. The difference, or error, can be attributed to unresolved tidal constituents, inertial currents or noise in the signal. The extracted solutions reflect only those current variations with a coherent phase and no assumptions are made about data outside the interval upon which the solutions are fit (*Pugh*, 1986).

The analysis of diurnal and semidiurnal constituents was conducted starting every six hours over 48 hour segments and produced a large number of independent estimates for each current record. The 48 hour period did not allow adequate separation of the O_1 and K_1 diurnal and the M_2 and S_2 semidiurnal constituents which had prevented by synodic periods of 13.661 and 14.765 days respectively. Therefore the major tidal constituents (O_1, K_1, P_1, Q_1, M_1, J_1; M_2, S_2, N_2, and K_2) were generalized as diurnal ($\omega \sim 1$ cycle per day) or semidiurnal ($\omega \sim 2$ cpd). Longer period constituents, such as the Lunar Long Period Mm and MSf, were removed by low pass filtering. Harmonics such as the Lunar Terdiurnal M_3 or Solar Terdiurnal S_3 were not considered due to the relatively small amplitude of these constituents when compared to the primary diurnal and semidiurnal constituents. Higher order harmonics were removed by the initial band pass

filtering. Inclusion of the inertial frequency ($\omega = 1.1$ cpd) as a known frequency provided a better fit of the least squares solutions and reduced error.

The complex demodulation program calculated the coefficients using a least squares approximation to the set of m equations with

$$u \text{ or } v = A_1 + A_2 \sin \omega(t - t_s) + A_3 \cos \omega(t - t_s)... \tag{17}$$

where ω is the angular frequency of the tidal constituent, t is the time of each hourly record and t_s is the time of the first data point of an entire current meter record. The number of terms can be expanded to A_{2n+1} to include all desired constituents n. For u velocities, data was placed in a single row matrix U. The coefficients of equation (17) are placed in matrix X. The following relationship was used to obtain the solutions to the set of equations represented by equation (17):

$$(U \times X^{-1}) \times (X \times X^{-1}) = AU$$

Similar calculations were done for the v velocities to create matrix AV. Once the coefficients A were determined (the values in matrices AU or AV), the amplitude and phase of each frequency component was calculated using

$$\text{Amp}_n = \sqrt{(A_{2n})^2 + (A_{2n+1})^2}$$

$$\theta = \arctan\left(\frac{A_{2n+1}}{A_{2n}}\right)$$

With these values, the current velocities can now be defined as

$$u \text{ or } v = \text{Amp}_n \sin(\omega(t - t_s) + \theta)$$

18

Diurnal and semidiurnal amplitude and phase were extracted from each current meter record using the complex demodulation technique. An example is provided in Figure 7.

2. Construction of Current Ellipses.

The amplitude and phase of clockwise (Q_c, θ_c) and anticlockwise (Q_{ac}, θ_{ac}) rotating vectors were computed using monthly averages of the component amplitude and phase vectors (U, θ_u) and (V, θ_v) obtained from complex demodulation using standard equations (*Pugh*, 1986):

$$Q_c = \frac{1}{2}\left[U^2 + V^2 - 2UV\sin(\theta_v - \theta_u)\right]^{\frac{1}{2}}$$

$$Q_{ac} = \frac{1}{2}\left[U^2 + V^2 + 2UV\sin(\theta_v - \theta_u)\right]^{\frac{1}{2}}$$

$$\theta_c = \arctan\left\{\frac{U\sin\theta_u + V\cos\theta_v}{U\cos\theta_u - V\sin\theta_v}\right\}$$

$$\theta_{ac} = \arctan\left\{\frac{U\sin\theta_u + V\cos\theta_v}{-U\cos\theta_u - V\sin\theta_v}\right\}$$

Using the rotary components, the dimensions of a current ellipse may be defined as

$$\text{Semi-major Axis} = Q_c + Q_{ac}$$

$$\text{Semi-minor Axis} = |Q_c - Q_{ac}|$$

$$\text{Orientation of Semi-major Axis (clockwise from North)} = \frac{\pi}{2} - \frac{1}{2}(\theta_{ac} + \theta_c)$$

Current rotation is clockwise if $Q_c > Q_{ac}$ and anticlockwise if $Q_{ac} > Q_c$. Sample ellipses are shown for mooring P2 during December 1989 (Figure 8).

19
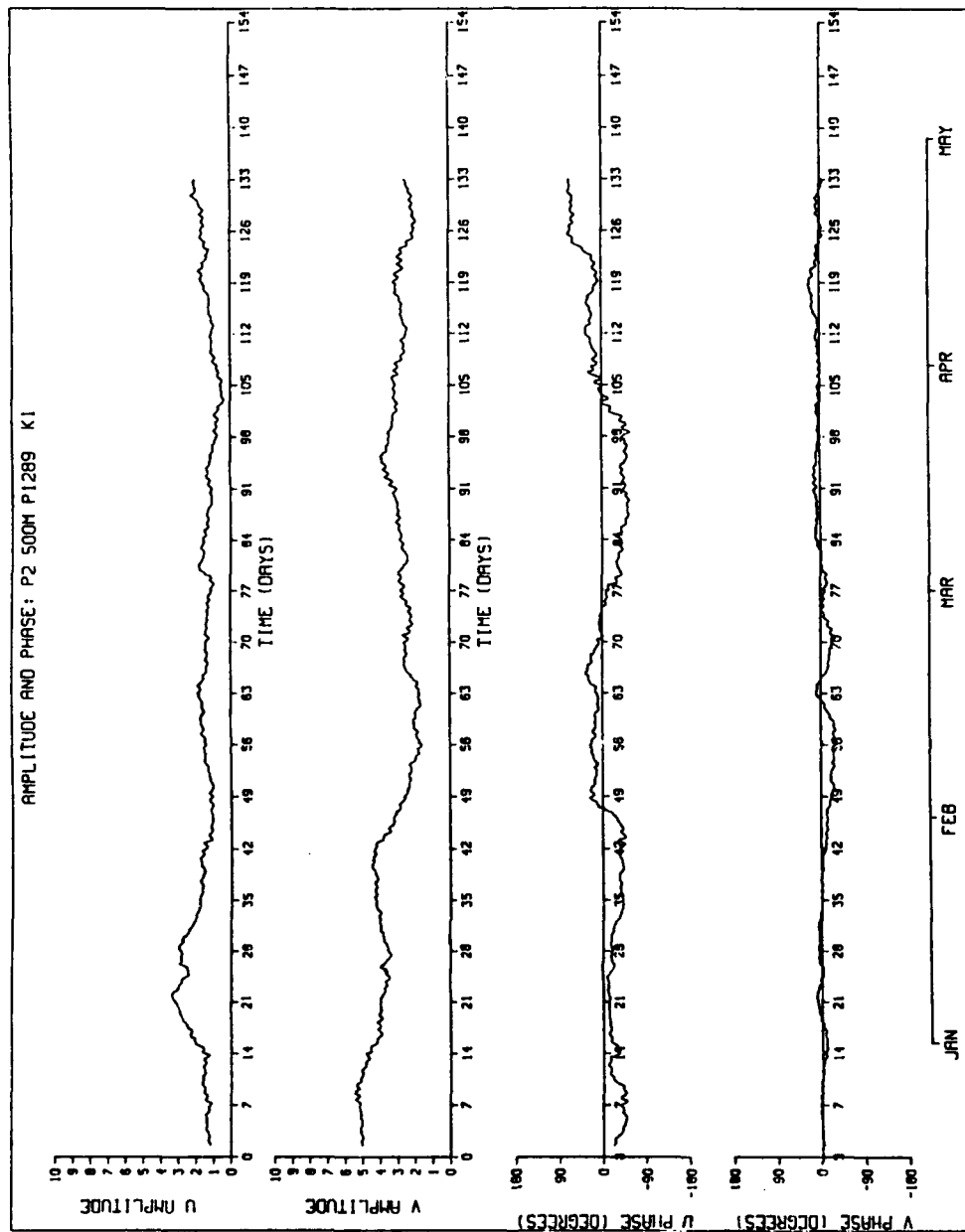
Figure 7. Complex Demodulation of the Diurnal Frequency at 500 m on Mooring P2: The first two time series plotted are amplitudes in cm sec^{-1} and the next two curves are the phases of the u and v diurnal velocity components in degrees relative to the beginning of each record.

20
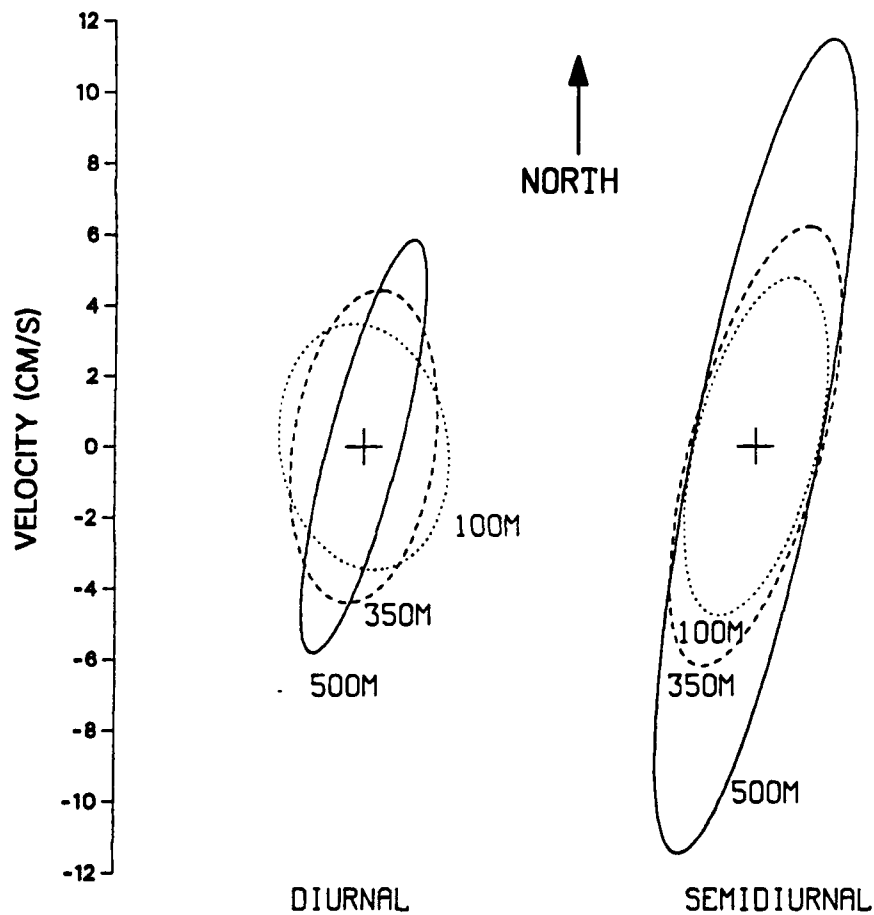
Figure 8.   **Tidal Current Ellipses:** Current ellipses are shown for diurnal and semidiurnal tidal currents at P2 for December 1989. North is towards the top of the page.

Current ellipses from different moorings and varying depths were evaluated by visual comparison of the ellipse orientation, size, eccentricity and rotation and by quantitative comparison of the energy represented by each ellipse. Energy was computed in units of cm^2 sec^{-2} by the addition of the squared dimensions of the semi-major and semi-minor axis.

C. SPECTRAL ENERGY ANALYSIS

To evaluate the energy present in the tidal currents, a program which computes the spectral characteristics of a time series was employed. The program, VCSPC3, was used to calculate the kinetic energy (KE) spectra as the total KE spectra for both the u and v velocities of a current meter record over one month periods. The program utilized a Cooley-Tukey fast fourier transform (FFT). One month records were divided into five sequential, equal length segments. A separate spectrum was computed for each segment and the five segments were then averaged to produce the total energy spectrum. A parabolic data window was used in the program to eliminate discontinuities at the beginning and end of records created because record lengths were not exact multiples of the periods of each wave present in the signal (*Bendat and Piersol*, 1986). The effect of the data window was to improve the resolution of the narrow spectral peaks in the tidal frequencies by reducing spectral side lobe leakage and associated distortion. No additional smoothing of the spectral estimates was done. The program calculated 95% confidence intervals using a Chi squared distribution.

Program VCSPC3 provided both graphical output and data listings. The plots show kinetic energy density in units of cm^2 sec^{-2} cpd^{-1} versus frequency in cpd. Confidence intervals are indicated by the separation of parallel horizontal lines above the horizontal axis. Distinct peaks were clearly seen at both the diurnal and semidiurnal frequencies of these plots (Figure 9).
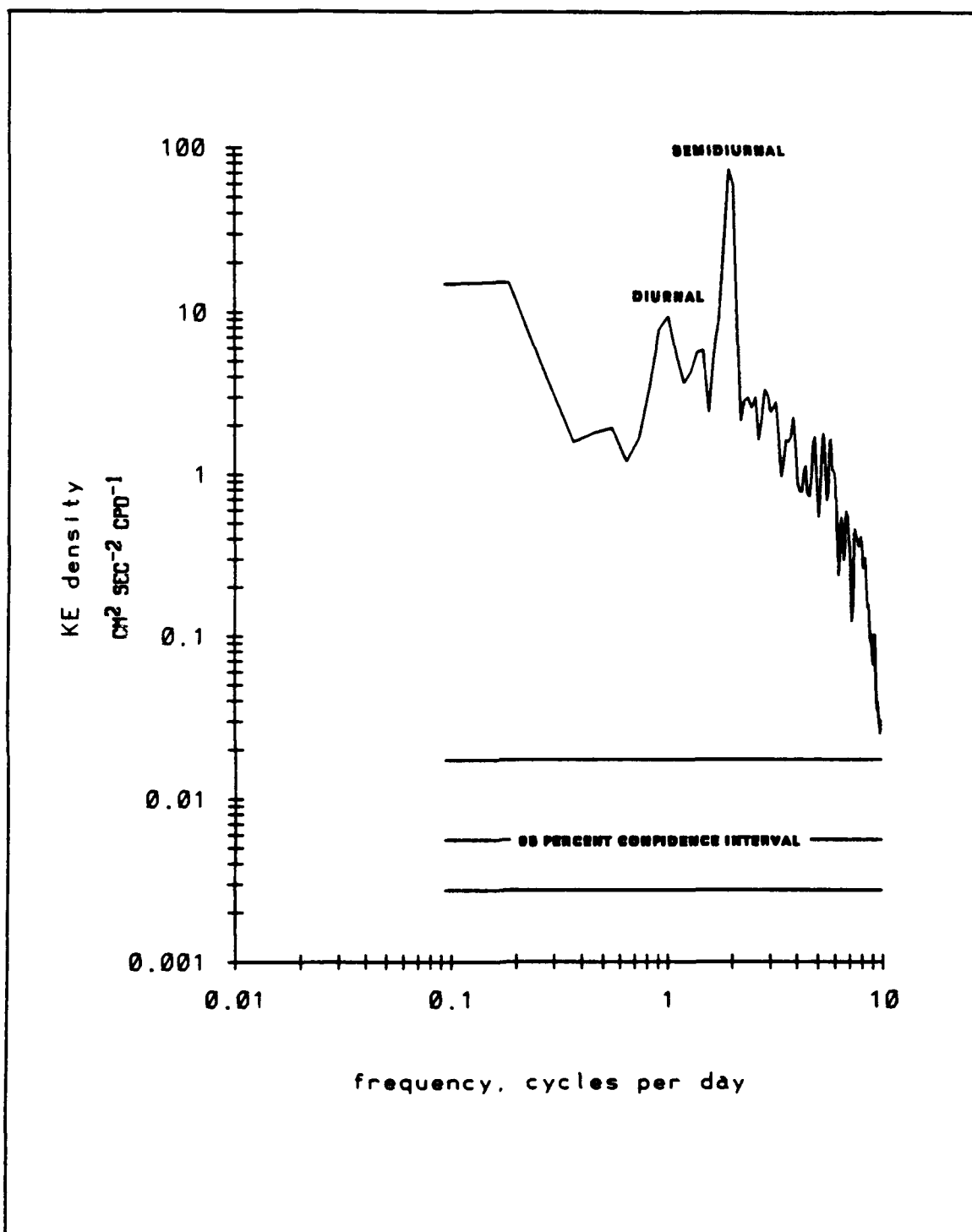
22

Figure 9. **Spectral Energy at P2:** A representative plot from the spectral analysis program is shown for a one month interval. The 95% confidence intervals is plotted below the curve.

The listings show spectral density at the diurnal and semidiurnal frequencies with a frequency resolution of 0.05 cpd and the associated 95 percent confidence intervals.

D. HYDROGRAPHIC DATA

A series of temperature (T), salinity (S), density (σ_t), geostrophic height (Φ), geostrophic velocity (V), and spiciness (π), values were plotted in contoured vertical sections which passed through the locations of moorings P2 and P3 (figures not shown). A level of no motion for the geostrophic velocity calculations was chosen at 1000 m except where bottom depths were less than 1000 m when the greatest common depth between stations was used. Brunt-Väisälä (or buoyancy) frequency N was computed for each cruise at the stations nearest moorings P2 and P3. Usually the CTD cast was within a few kilometers of the moorings' assigned position. Values for N were determined by

$$N^2 = g \left[-\frac{1}{\rho} \frac{\partial \rho}{\partial z} \right] \tag{18}$$

Values of ρ used in equation (18) were computed using the International Equation of State 1980 for seawater (*Millero and Poisson*, 1981) using S, T and P values from the CTD cast and were smoothed by center averaging over 10 m increments. Calculations of N^2 used $\Delta z = 10$ m. The results from each CTD cast were plotted as a vertical profile of N^2 against depth. Most N^2 profiles revealed the main pycnocline at depths between 50 m and 200 m. The highest value of N, 2.147×10^{-3} cps (a 7.76 minute period), was found near the main pycnocline. Minimum N values were found at the bottom of each cast with values near 2.344×10^{-4} cps (a 71.01 minute period) and were assumed to be constant from the deepest calculated value to the sea floor.

Profiles of the maximum trapping frequency $\omega_c = N\sin\alpha$ were constructed with the trapping frequency plotted in units of cpd against depth in meters. The possibility of

bottom trapping at any particular CTD station is best indicated by the magnitude of the

maximum trapping frequency calculated over the lowest 10 m of CTD data (Figure 10).

The deepest calculated ω_c, typically 50 m off the bottom, was extrapolated to the bottom

using the assumption that N^2 remained constant. Any wave with a frequency less than

or equal to ω_c may be trapped. When ω_c is greater than 2.0 cpd, trapping may occur

at both diurnal and semidiurnal frequencies. When ω_c is less than 1.0 cpd, no trapping

of tidal currents should be expected.

BRUNT-VAISALA FREQUENCY PROFILE   Nsinα FREQUENCY PROFILE

N**2 (10E-06)

| 0 | 5 | 10 | 15 | 20 | 25 | 30 | 35 | 40 | 45 | 50 |

CYCLES PER DAY

| 0 | 5 | 10 | 15 | 20 |

DEPTH (METERS)

PROFILE ID: CUMARSO STA 11 MOORING P3
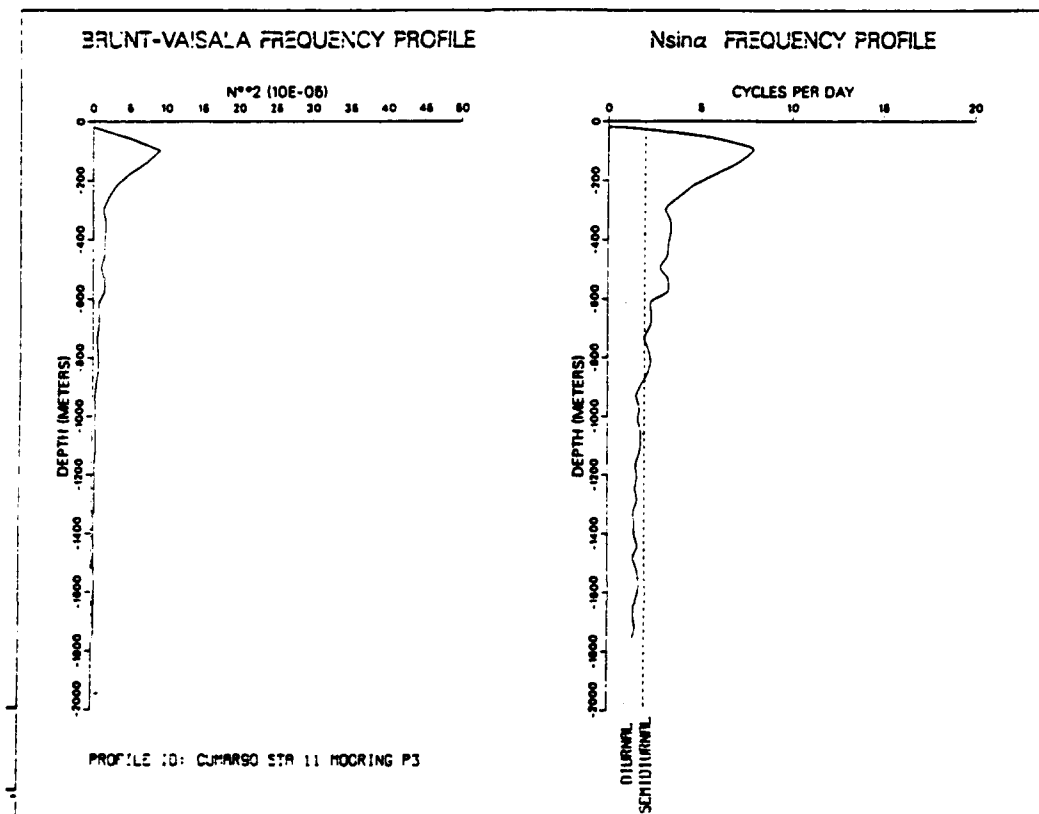
DIURNAL
SEMIDIURNAL

Figure 10.   Brunt-Väisälä Frequency and Trapping Frequency Profiles: N^2 and $N \sin \alpha$ are plotted versus depth using hydrographic data obtained near P3 in March 1990.

26

IV. RESULTS

A. CURRENT ELLIPSES

Monthly averaged tidal current ellipses were constructed using the amplitudes and phases obtained from the complex demodulation of current meter records (Figures 11 to 14). The plotted ellipses display a great deal of variability in their size, orientation and direction of rotation. The size and energy represented by the current ellipses was found to be greatest for both tidal frequencies at the deepest current meter of mooring P2.

1. Diurnal Current Ellipses

Diurnal current ellipses for mooring P2 were constructed for seventeen consecutive months (Figures 11 and 12). The energy represented by the ellipses was calculated using the sum of the squared axis lengths to compute kinetic energy in units of $cm^2 sec^{-2}$. At the 100 m level the average energy of the ellipses was 18.0 $cm^2 sec^{-2}$. The direction of rotation of 76% of these ellipses was counterclockwise. At 350 m, the average energy dropped to 14.5 $cm^2 sec^{-2}$ with 70% of the ellipses rotating counterclockwise. At 500 m, the average ellipse energy increased to 22.3 $cm^2 sec^{-2}$ with 65% rotating counterclockwise. The diurnal current ellipses were larger and more energetic at 500 m than at 350 m for each of the seventeen months analyzed and there were twelve months when more energy was present at 500 m than at 100 m. During July 1989 the diurnal current rotation at all three P2 current meters was clockwise and there were eight months when the rotation at three depths was uniformly counterclockwise.

The current meter records for six months were used to construct diurnal current ellipses at mooring P3 (Figure 12). At the 100 m level the average energy represented by the ellipses was 25.1 $cm^2 sec^{-2}$ with 66% of the ellipses rotating counterclockwise.
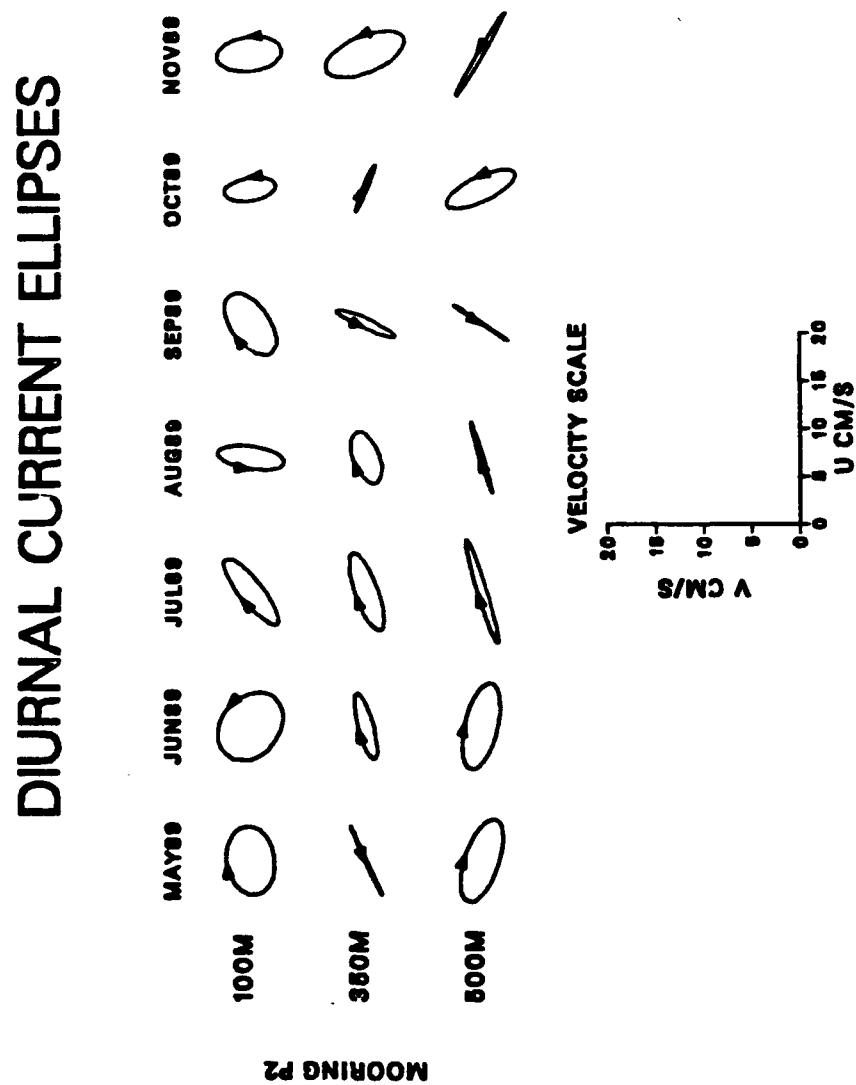
Figure 11. Diurnal Current Ellipses from May 1989 to November 1989 at Mooring P2: Horizontal ellipses are shown with north up and the direction of rotation indicated by arrows. A velocity scale is indicated at the bottom.

28

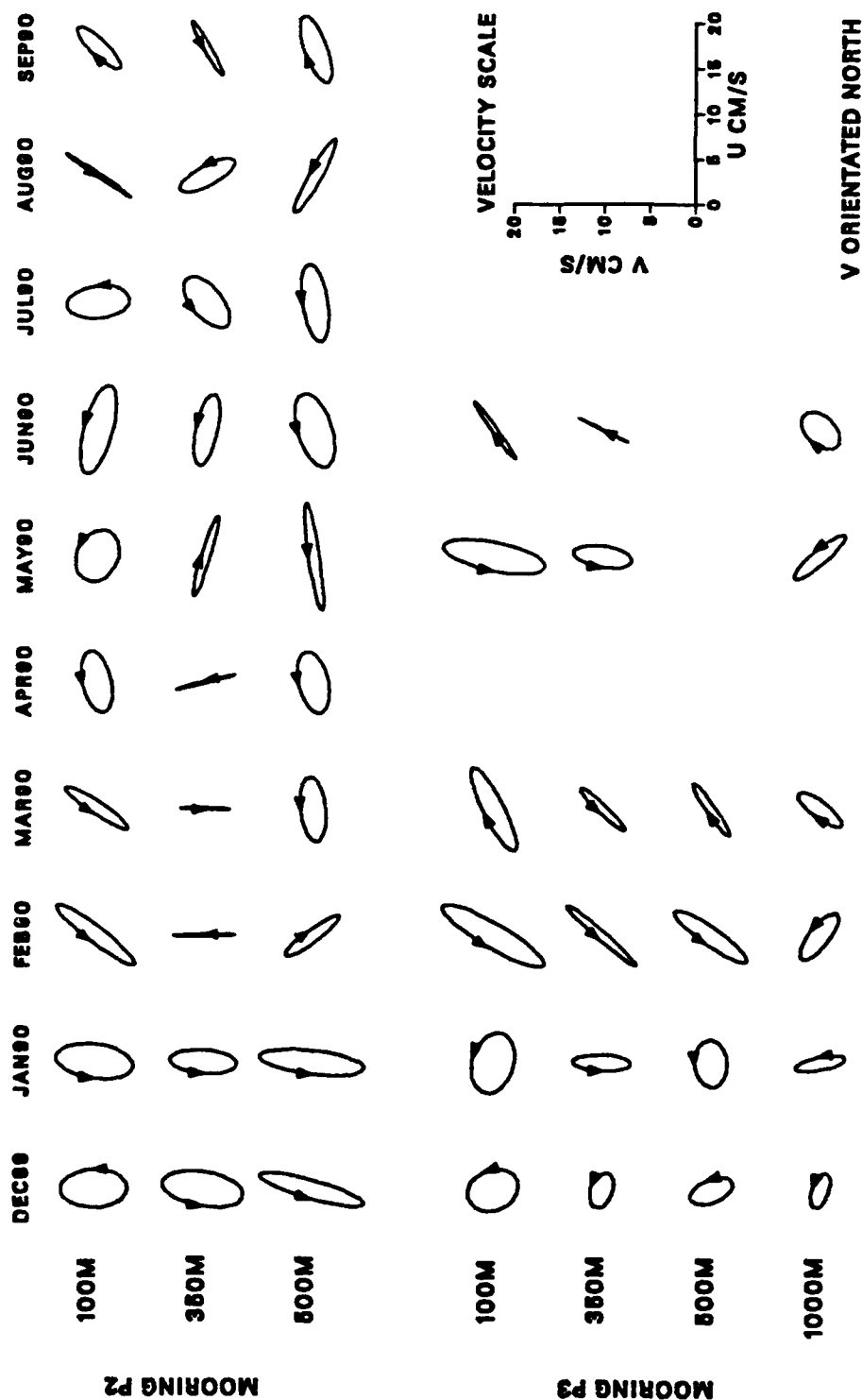Figure 12. Diurnal Current Ellipses from December 1989 to September 1990 at Moorings P2 and P3: Details are as in Figure 11.

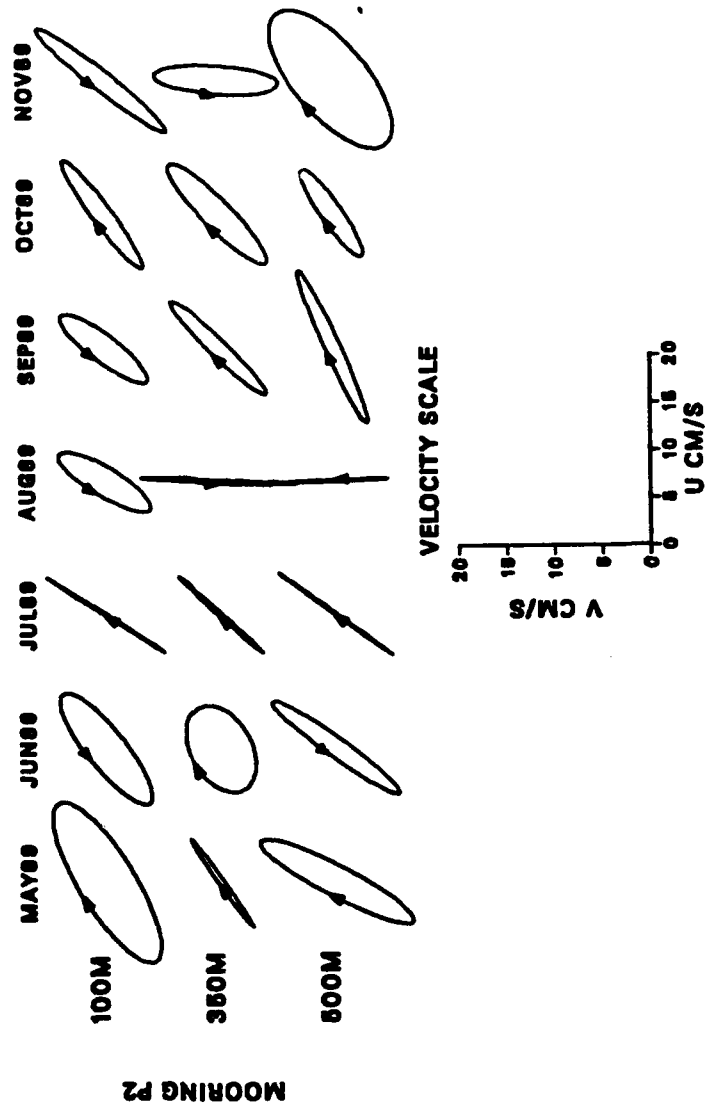Figure 13. Semidiurnal Current Ellipses from May 1989 to November 1989 at Moorings P2 and P3: Details are as in Figure 11.
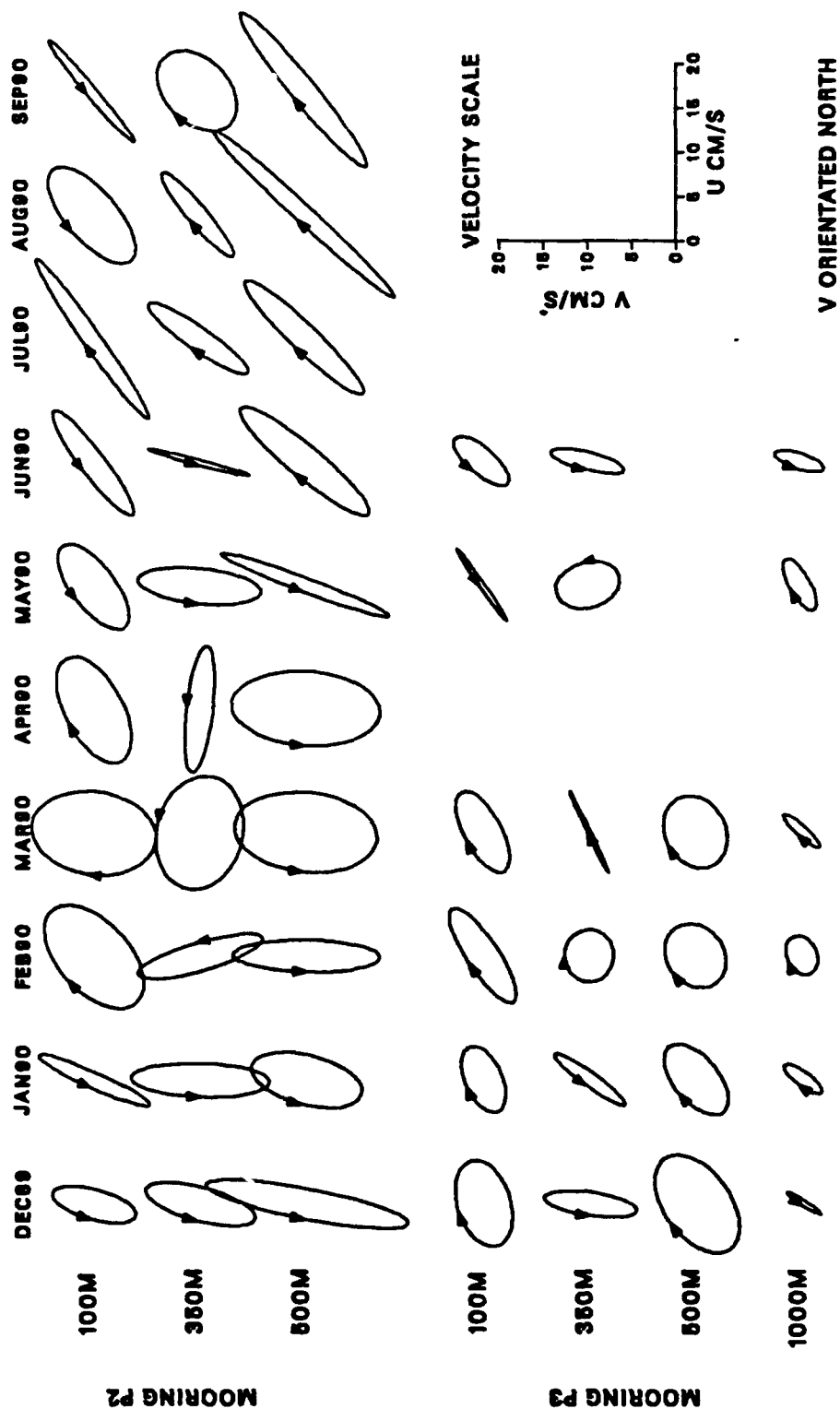
Figure 14. Semidiurnal Current Ellipses from December 1989 to September 1990 at Mooring P2 and P3: Details are as in Figure 11.

31

At 350 m, the average energy dropped to 12.4 cm² sec⁻² . At 500 m, four months were analyzed and resulted in an average energy of 13.5 cm² sec⁻² with 75% rotating counterclockwise. The smallest ellipses and lowest energy (9.5 cm² sec⁻²) were found at 1000 m with 66% of the ellipses rotating counterclockwise. The ellipses were larger and contained more energy at 500 m than did those at either 350 m or 1000 m. There were four months when the current rotation at each P3 current meter was counterclockwise.

The bathymetric contours at mooring P2 are oriented at approximately 005 °T and the average orientation of the 500 m diurnal tidal current ellipses at P2 was 049° T. The semi-major axis of the diurnal ellipses crossed the isobaths a mean relative angle of 44°. At mooring P3 the bathymetry is oriented at 020° T. The average orientation of diurnal tidal ellipses at 1000 m was 074° T and the semi-major axis of these ellipses crossed the isobaths at a mean relative angle of 54°.

2. Semidiurnal Current Ellipses.

The semidiurnal current ellipses at P2 and P3 were larger and more energetic than those at diurnal frequencies. The orientation of the semidiurnal ellipses was less variable than the diurnal ellipses with almost all of them oriented in a north-northeast direction.

At mooring P2, the seventeen month average energy represented by the ellipses at 100 m was 59.1 cm² sec⁻². The rotation of 58% of these ellipses was counterclockwise. At 350 m, the average energy decreased to 48.2 cm² sec⁻² and 52% of the currents ro-

tated counterclockwise. At 500 m the average energy increased to 85.4 cm² sec⁻² with 47% of the ellipses displaying counterclockwise rotation. The semidiurnal currents displayed the same trends exhibited by the diurnal current ellipses where the largest ellipses and greatest energies were found at the deepest level and the smallest ellipses and least energy was at 350 m. The rotation of semidiurnal current ellipses at P2 was clockwise

32

at all three current meters during four months and counterclockwise during four other months. The remaining nine months contained ellipses with opposing rotation.

The semidiurnal current ellipses at mooring P3 were notably smaller than those at P2. The average energy represented by the ellipses at 100 m was 28.4 cm² sec⁻² with 66% rotating clockwise. At 350 m the average energy decreased to 22.7 cm² sec⁻² with 66% of the currents rotating counterclockwise. A four month average at 500 m resulted in an average semidiurnal energy of 34.5 cm² sec⁻² with all four ellipses rotating clockwise. At 1000 m the average energy was only 8.3 cm² sec⁻². At this level, 66% of the ellipses rotated clockwise. Like the diurnal currents at P3, the semidiurnal currents were greatest at 500 m. The smallest ellipses and least energy was at the 1000 m level. At mooring P3 two of the six months analyzed had semidiurnal currents at four depths rotating in a clockwise direction and there was one month when the rotation was counterclockwise at each depth.

The average orientation of 500 m semidiurnal current ellipses at P2 was 030° T and the isobaths were crossed at an angle of 25°. The average orientation of 1000 m semidiurnal current ellipses at P3 was 043° T and the semi-major axis crossed the isobaths at 23°.

B. ENERGY PROFILES

Vertical profiles of energy at both the diurnal and semidiurnal frequencies (Figures 15 and 16) were constructed for each month using the output from the spectral analysis program. These plots contain information similar to that of the tidal current ellipses expressed in a different format. At P2 the highest energy levels were at the deepest current meter for both frequencies. The energy levels at P3 show low energy levels at the deeper current meters.
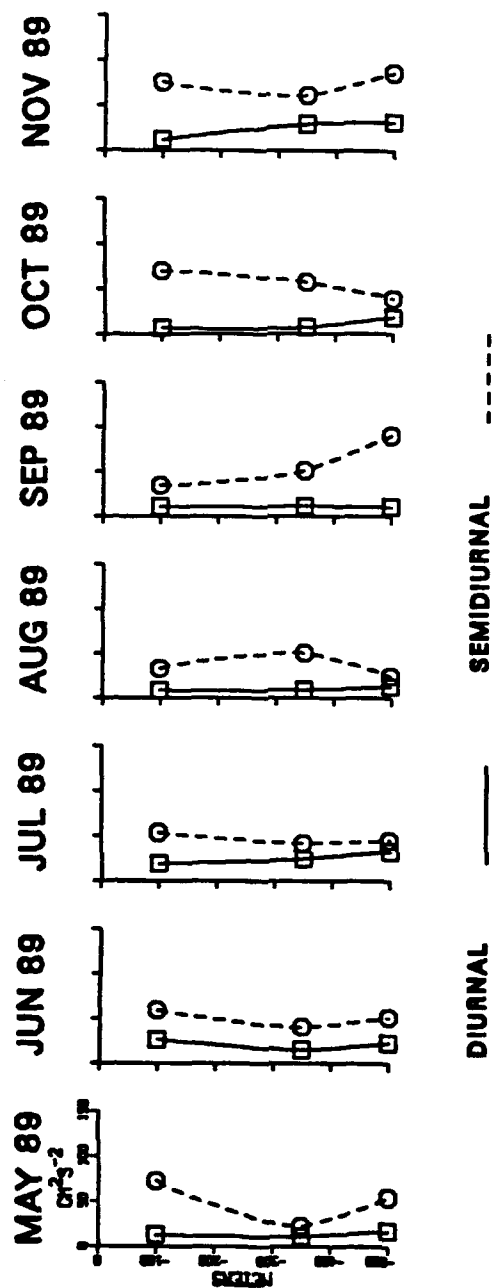
Figure 15. Spectral Energy Profiles from May 1989 to November 1989 at Mooring
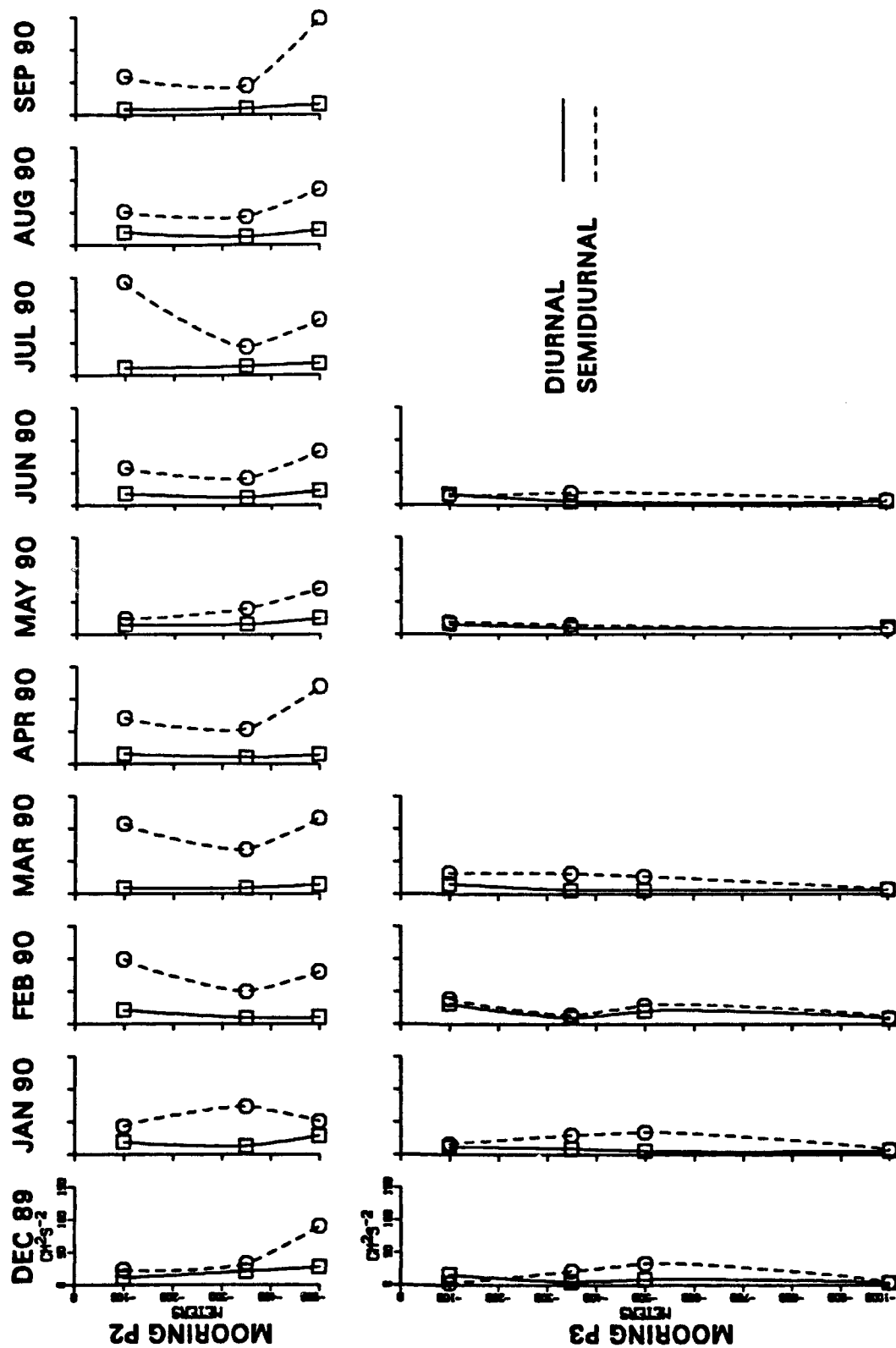P2: All plots are scaled identically.

Figure 16.   Spectral Energy Profiles from December 1989 to September 1990 at
Moorings P2 and P3:   All plots are scaled identically.

35

1. Diurnal Energy Profiles

At mooring P2 the average monthly diurnal energy levels were 13.9 cm^2 sec^{-2} at 100 m, 13.4 cm^2 sec^{-2} at 350 m and 20.2 cm^2 sec^{-2} at 500 m. The energy at 500 m exceeded that at 350 m for each of the seventeen months analyzed except September 1989. The energy at 500 m was also higher than that at 100 m except for the months of June 1989, February 1990 and April 1990. The curves plotted in Figures 15 and 16 exhibit a 'C' shape with minimum energy levels typically found at a depth of 350 m.

Diurnal energy at P3 was greatest near the surface. Average monthly values were 17.3 cm^2 sec^{-2} at 100 m, 7.2 cm^2 sec^{-2} at 350 m 9.7 cm^2 sec^{-2} at 500 m and 9.8 cm^2 sec^{-2} at 1000 m. The curves plotted below 100 m are nearly uniform and show virtually no amplification of energy toward the bottom.

2. Semidiurnal Energy Profiles

The semidiurnal current energy levels at P2 were likewise greatest at the deepest current meters. The same 'C' shaped curve observed with diurnal currents, with a minimum energy at 350 m, was exhibited by the semidiurnal currents. Average monthly values of 63.1, 47.6, and 77.4 cm^2 sec^{-2} were found at 100 m, 350 m and 500 m respectively. The energy at 500 m was greater than that at 350 m for fourteen of the seventeen months analyzed. The energy at 500 m exceeded that at 100 m for nine of the seventeen months.

At P3, the average semidiurnal energy levels were fairly consistent until dropping off sharply at 1000 m. Values of 20.1, 21.3, 30.3 and 7.3 cm^2 sec^{-2} were found at 100 m, 350 m, 500 m and 1000 m. No bottom amplification of semidiurnal energy was evident at P3.

C. TEMPORAL VARIABILITY

The same data used to plot the vertical profiles were used to create time series showing the change of energy at each depth for the two moorings. Diurnal bottom

36

trapping was evident at P2, with energy at 500 m greater than the energy at 350 m for the entire seventeen month period analyzed (Figure 17). Bottom trapping was always present and was most pronounced during July - August 1989, October 1989 - January 1990 and May - September 1990 when the energy at 500 m exceeded that of any other depth. The magnitude of the diurnal energy at 500 m was statistically greater than 350 m or 100 m at 95 percent confidence for the period October 1989 through January 1990. At mooring P3 no diurnal bottom trapping was indicated by the energy at 350 m, 500 m or 1000 m (Figure 18). Diurnal energy did not increase toward the bottom and the energy near the surface, at 100 m, was always greater than at deeper current meters.

Bottom trapping of semidiurnal energy occurred at P2 for fourteen of seventeen months when the energy at 500 m exceeded the energy at 350 m (Figure 19). In addition, the energy at 500 m was greater than 100m for nine of the seventeen months analyzed. Bottom trapping at 500 m was statistically significant using a 95 percent confidence interval for September 1989, December 1989, April - May 1990 and September 1990. At P3 no semidiurnal trapping was evident and the energy at 1000 m was less than at any other depth for five of the six months analyzed (Figure 20).

D. APPLICATION OF TRAPPING THEORY

The size of the current ellipses and energy distribution at each depth suggest that an amplification of energy occurs near the bottom of mooring P2. A similar pattern was not obvious at P3. To compare observed motions to theoretical trapped waves an exponential curve, representing the decay of trapped energy, was compared to the observed profile of kinetic energy. The theoretical curves were constructed using equation (12) with κ given by equation (16).

1. Trapping Scales and Decay Curves

At mooring P2 the maximum trapping frequency is exactly equal to the diurnal frequency ($\omega_c = 1$ cpd) when, by equation (7), $N = 1.930 \times 10^{-4}$ cps . Using $H = 800$ m
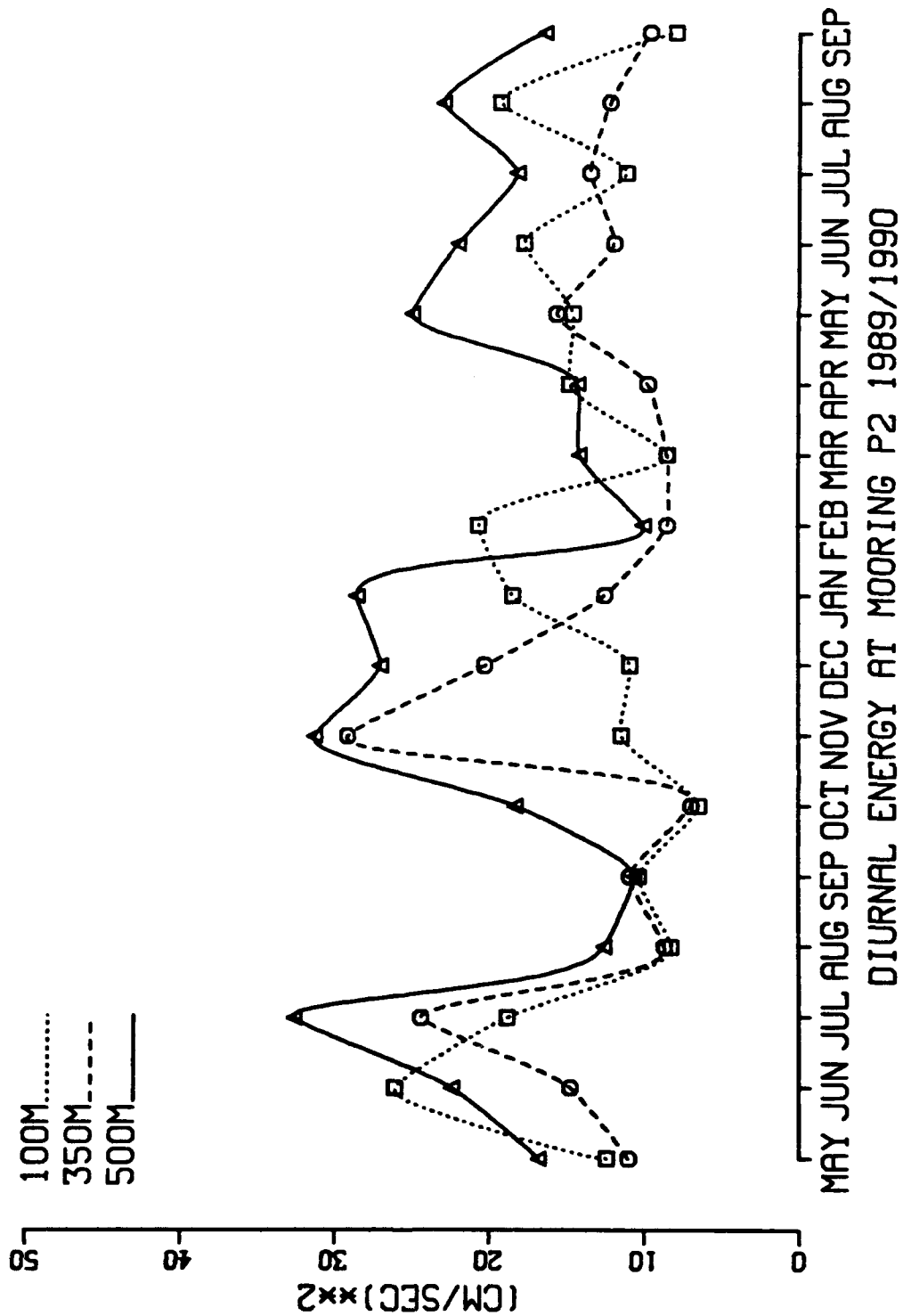
Figure 17. **Time Series of Diurnal Energy at Mooring P2:** The temporal variability of kinetic energy is shown with curves representing the energy levels at current meter depths.
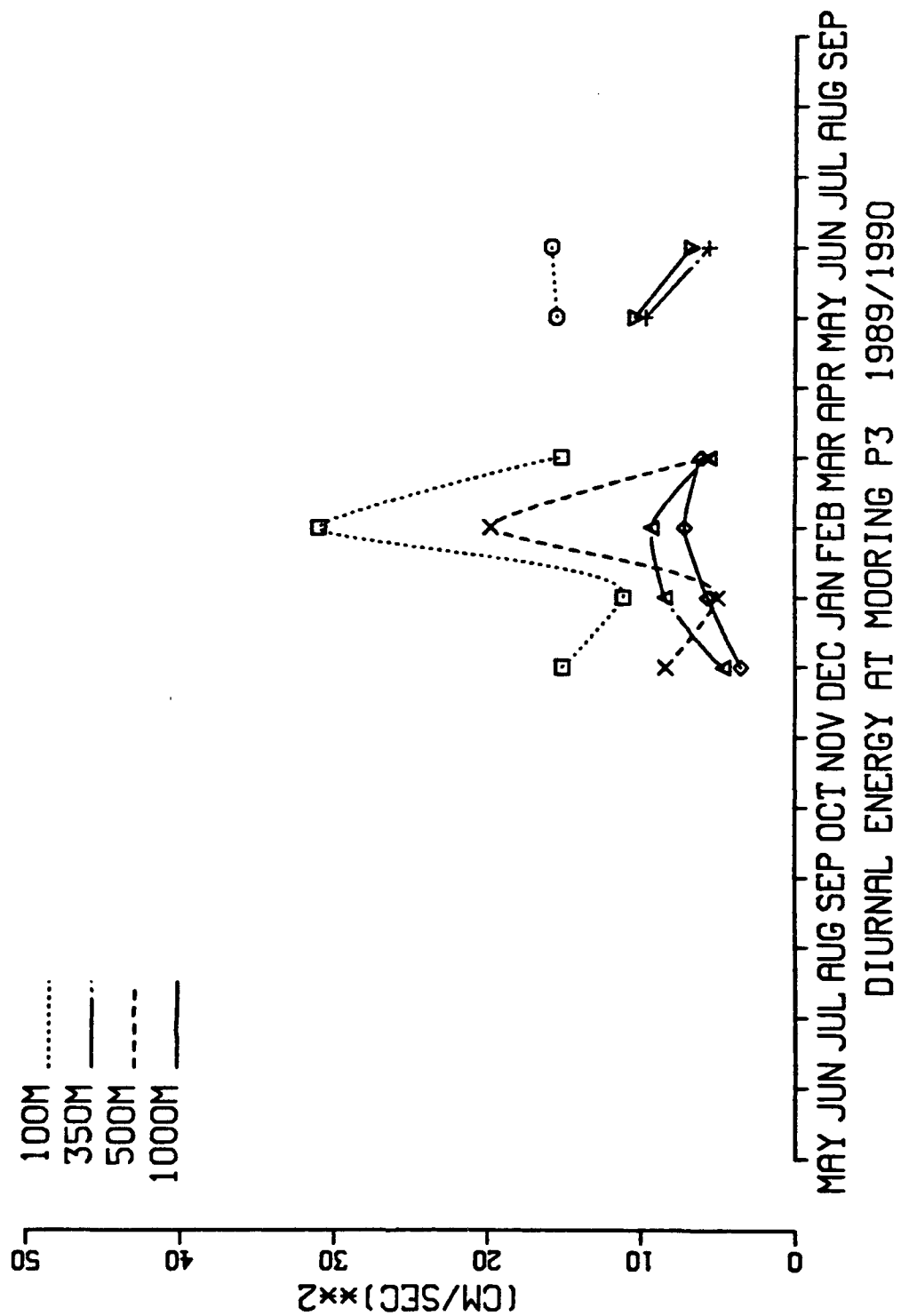
38

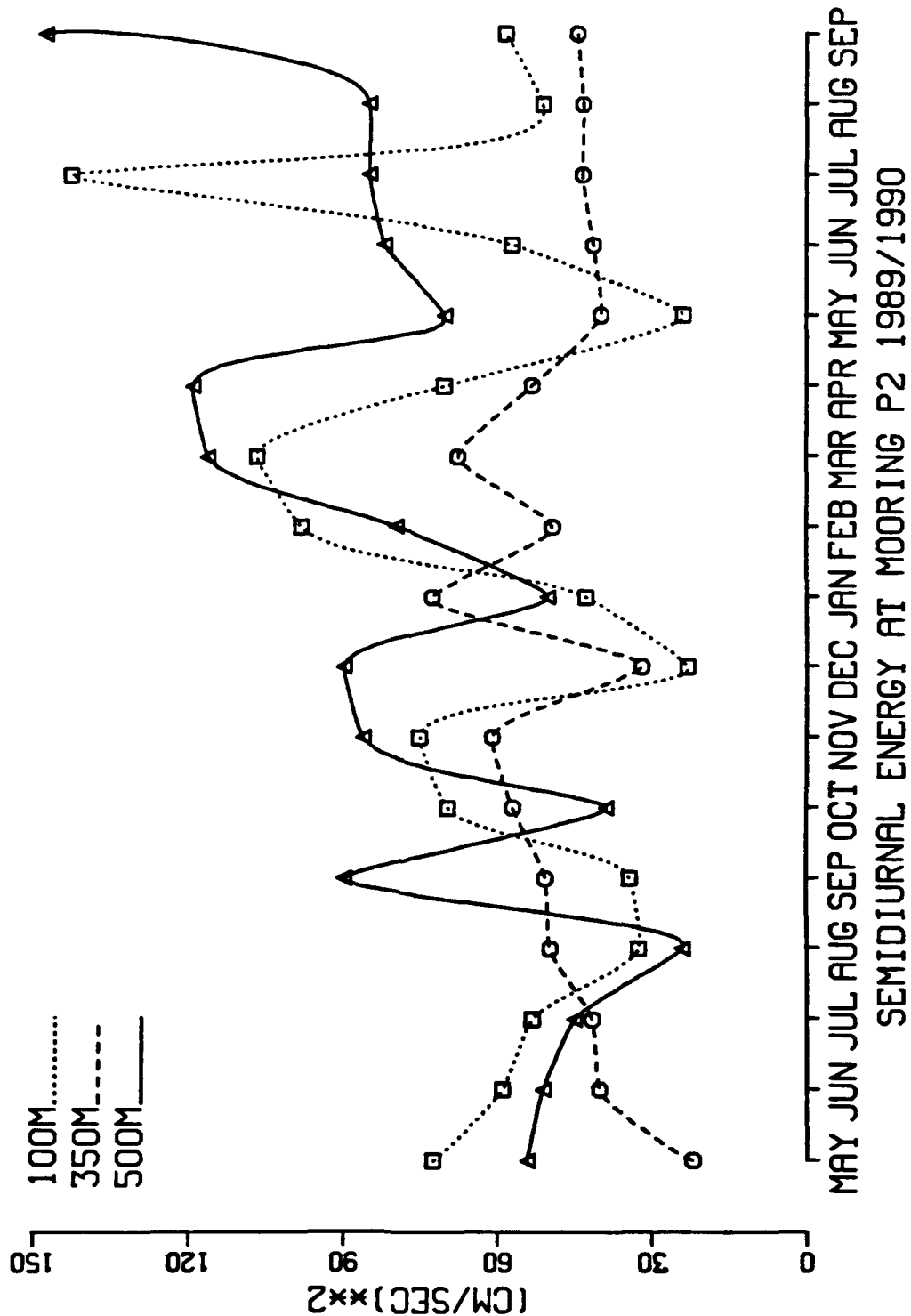Figure 18. Time Series of Diurnal Energy at Mooring P3: As indicated in Figure 17.

Figure 19. Time Series of Semidiurnal Energy at Mooring P2: As indicated in Figure 17.
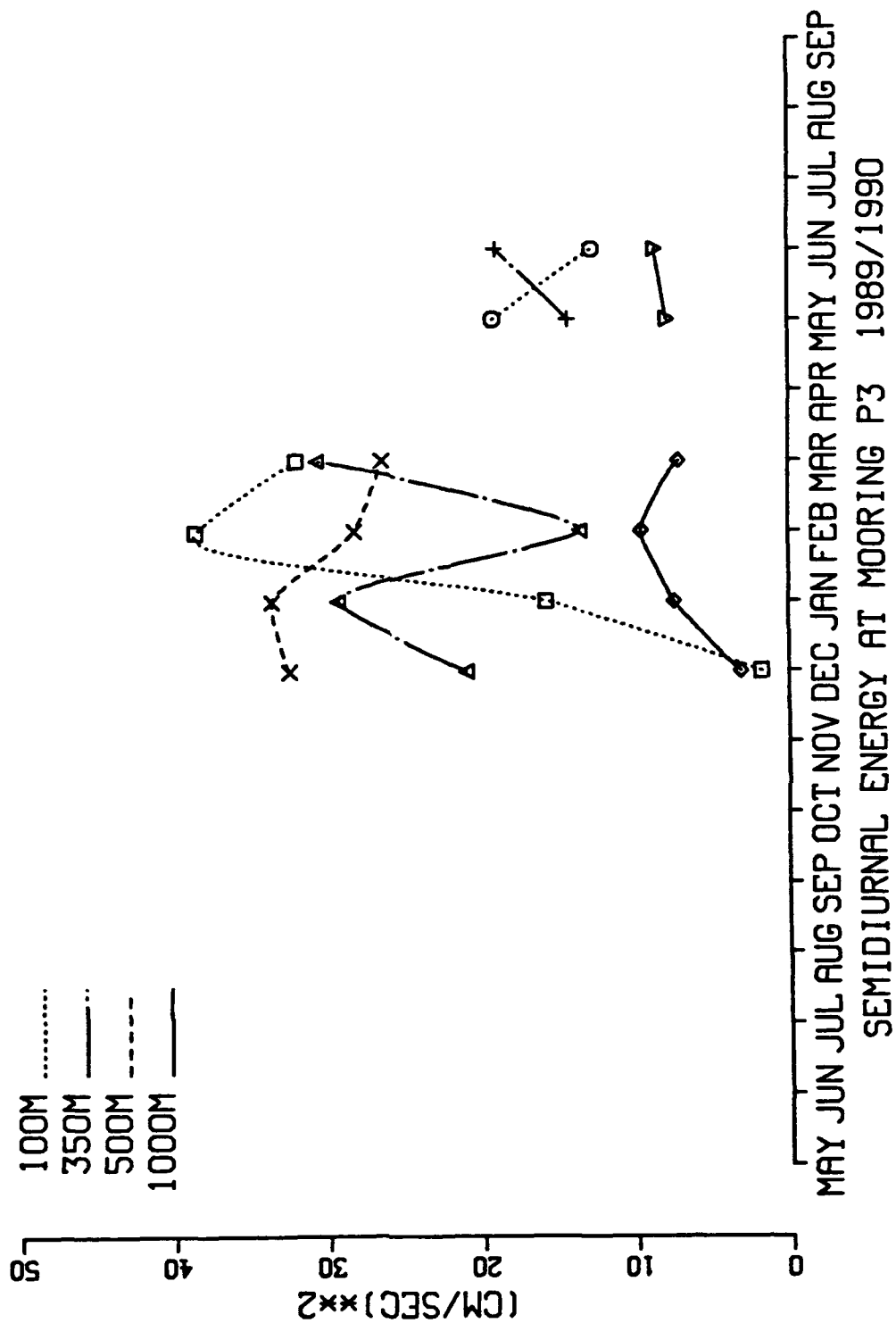
40

Figure 20. Time Series of Semidiurnal Energy at Mooring P3: As indicated in Figure 17.

and $f = 1.375 \times 10^{-5}$ cps in equation (16) results in a trapping coefficient of $\kappa = 3.3116 \times 10^{-3}$ m^{-1}. The horizontal length scale of this wave is $L = \dfrac{2\pi}{k} = 26.632$ km. Similar calculations were conducted for the first five baroclinic modes at both P2 and P3 for diurnal and semidiurnal trapping using N values determined by equation (7). The coefficients are tabulated in Tables 3 and 4.

Table 3. TRAPPING COEFFICIENTS AT MOORING P2

$\omega_c = 1$ cpd	$\omega_c = 2$ cpd
$\kappa_1 = 3.311 \times 10^{-3}$ m^{-1}	$\kappa_1 = 1.472 \times 10^{-3}$ m^{-1}
$\kappa_2 = 6.622 \times 10^{-3}$ m^{-1}	$\kappa_2 = 2.943 \times 10^{-3}$ m^{-1}
$\kappa_3 = 9.934 \times 10^{-3}$ m^{-1}	$\kappa_3 = 4.415 \times 10^{-3}$ m^{-1}
$\kappa_4 = 1.321 \times 10^{-2}$ m^{-1}	$\kappa_4 = 5.887 \times 10^{-3}$ m^{-1}
$\kappa_5 = 1.652 \times 10^{-2}$ m^{-1}	$\kappa_5 = 7.358 \times 10^{-3}$ m^{-1}

Table 4. TRAPPING COEFFICIENTS AT MOORING P3

$\omega_c = 1$ cpd	$\omega_c = 2$ cpd
$\kappa_1 = 6.622 \times 10^{-3}$ m^{-1}	$\kappa_1 = 2.949 \times 10^{-3}$ m^{-1}
$\kappa_2 = 1.324 \times 10^{-2}$ m^{-1}	$\kappa_2 = 5.887 \times 10^{-3}$ m^{-1}
$\kappa_3 = 1.986 \times 10^{-2}$ m^{-1}	$\kappa_3 = 8.830 \times 10^{-3}$ m^{-1}
$\kappa_4 = 2.643 \times 10^{-2}$ m^{-1}	$\kappa_4 = 1.177 \times 10^{-3}$ m^{-1}
$\kappa_5 = 3.331 \times 10^{-2}$ m^{-1}	$\kappa_5 = 1.476 \times 10^{-2}$ m^{-1}

For the baroclinic modes, the trapping coefficients in Tables 3 and 4 were used to produce a vertical trapping scale. The trapping scale (or e-folding scale) indicates the height off the bottom where the energy of a trapped wave decayed by a factor of e^{-1}. Most of the trapped energy for each wave was contained in a bottom layer with a thickness (determined by the trapping scale) indicated in Table 5. Note that the two deepest current meters at P2 (located 450 m and 300 m from the bottom) fell within this

layer but the lowest instrument at P3 (located 800 m from the bottom) did not. For higher modes trapping is stronger, trapping scales are smaller and energy decays more rapidly from the bottom.

Table 5. TRAPPING SCALES AT MOORINGS P2 AND P3

Mooring	$\omega_c = 1$ cpd	$\omega_c = 2$ cpd
P2	302 m	679 m
P3	151 m	339 m

Using the appropriate trapping coefficient, exponential decay curves for each mooring were constructed which represent the first two baroclinic modes at diurnal and semidiurnal frequencies at moorings P2 and P3 (Figures 21 and 22). Similar curves were fit to observed spectral energy profiles to determine if the vertical energy distribution off Point Sur indicated the presence of bottom trapped waves. The curves were constructed using N values determined from CTD data whenever the diurnal or semidiurnal frequencies were less than the maximum trapping frequency.

2. Analysis of Bottom Trapping

CTD data from each of the hydrographic cruises in Table 2 was analyzed to see if bottom trapping was possible at P2 or P3 at diurnal or semidiurnal frequencies using the criteria that $\omega_c = N \sin \alpha$ must be equal to or greater than the tidal frequencies. Each CTD cast taken at a mooring site was assumed to be representative of the averaging interval used to compute the spectral estimates (one month).

When bottom trapping was possible, theoretical decay curves were constructed using observed values of H, N, and appropriate trapping coefficients (κ). The curves were compared to the observed energy levels obtained from spectral analysis by matching the curves at the level of the deepest current meter (500 m at P2) and comparing the theoretical and observed energy at other (100 m and 350 m at P2) levels. When the

43
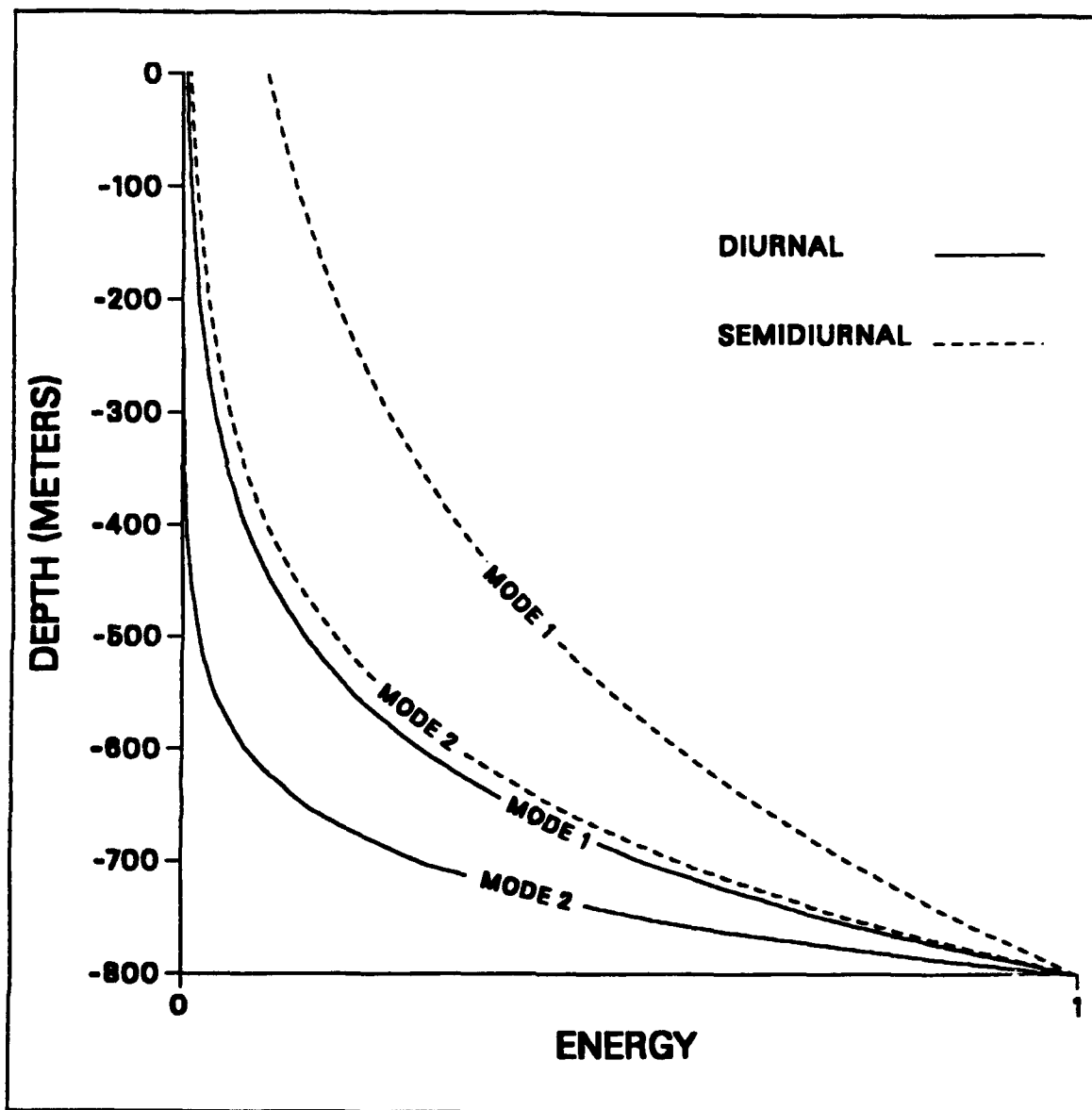
Figure 21. Theoretical Trapping Profiles at Mooring P2: The exponential decay of trapped energy (with arbitrary units) is illustrated for the first and second modes at tidal frequencies.

modeled energy fell within the 95 percent confidence intervals of the observations, the change of energy with depth was considered to be consistent with bottom trapped waves.

The buoyancy frequencies N, maximum trapping frequencies ω_c and trapping coefficients κ, for each month when data were available are tabulated in Table 6. The
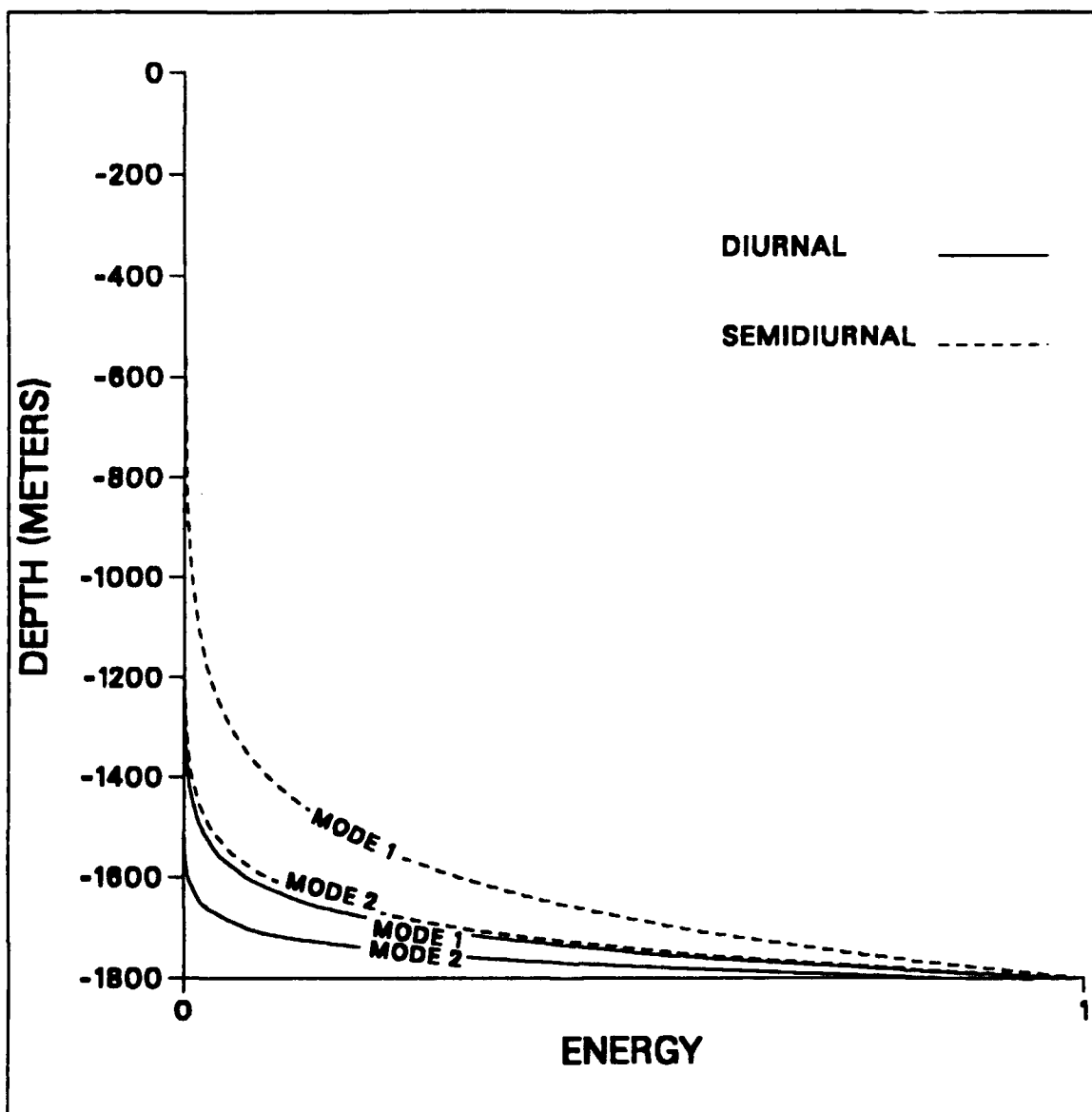
Figure 22. Theoretical Trapping Profiles at Mooring P3: The exponential decay of trapped energy (with arbitrary units) is illustrated for the first and second modes at tidal frequencies.

maximum trapping frequency ω_c at P2 exceeded the diurnal frequency ($\omega = 1.0$ cpd) each of the eight months. The maximum trapping frequency exceeded the semidiurnal frequency ($\omega = 2.0$ cpd) except for the month of January 1990 ($\omega_c = 1.22$ cpd).

Table 6. OBSERVED BUOYANCY FREQUENCIES, TRAPPING FREQUENCIES AND MODE 1 TRAPPING COEFFICIENTS AT MOORING P2

Month	N (cpd)	ω_c (cpd)	$\kappa_{Diurnal}$ (m^{-1})	$\kappa_{Semidiurnal}$ (m^{-1})
MAY 89	66.2	3.97	3.30555 x 10^{-3}	6.61116 x 10^{-3}
JUL 89	43.0	2.57	3.30556 x 10^{-3}	6.61127 x 10^{-3}
SEP 89	39.4	2.36	3.30557 x 10^{-3}	6.61130 x 10^{-3}
NOV 89	34.7	2.08	3.30558 x 10^{-3}	6.61137 x 10^{-3}
JAN 90	20.3	1.22	3.30564 x 10^{-3}	No Trapping
MAR 90	51.8	3.10	3.30556 x 10^{-3}	6.61121 x 10^{-3}
MAY 90	38.7	2.32	3.30557 x 10^{-3}	6.61131 x 10^{-3}
JUN 90	55.7	3.34	3.30556 x 10^{-3}	6.61120 x 10^{-3}
AVERAGE	**43.7**	**2.62**	**3.30557 x 10^{-3}**	**6.61126 x 10^{-3}**

The diurnal energy distribution at P2 (Figures 23 and 24) agreed with the modeled decay for seven of the eight months. During January 1990, the observed energy at 350 m was less than indicated by theory. The theoretical curves, extrapolated to a depth of 800 m, indicated an average kinetic energy level of 40.5 cm^2 sec^{-2} trapped at the sea floor.

The maximum trapping frequency ω_c at P2 exceeded the semidiurnal frequency ($\omega_c = 2.0$ cpd) during seven of the eight months. The observed energy at 100 m during May 1989 was higher than was modeled by matching the theoretical curve to the 500 m observation. The modeled curve fell within the 95 percent confidence intervals for the six remaining months. Extrapolation of the theoretical curve to 800 meters produced an average kinetic energy level of 310.0 cm^2 sec^{-2} at the bottom over the time period studied.

The buoyancy frequency calculated over the deepest 10 m of CTD data ranged from 20.3 cpd to 66.2 cpd and the magnitude of the maximum trapping frequency, which was proportional to N, ranged from 1.22 cpd to 3.97 cpd. The fluctuations of N had a

much smaller effect on the trapping coefficients. The diurnal trapping coefficient at P2 varied only 9.0×10^{-8} m^{-1}. The semidiurnal trapping coefficient had a range of only 2.1×10^{-7} m^{-1}. The consistent trapping coefficients produced nearly identical trapping scales at P2. The diurnal trapping scale (defined by the e-folding scale) was 302 m and the semidiurnal trapping scale was 151 m for each of the eight months analyzed.

The diurnal energy distribution at P3 did not have a profile indicative of bottom trapped waves. Since the maximum trapping scale for a diurnal wave at P3 was approximately 151 m and the deepest current meter at P3 was 800 m above the sea floor, any energy from a trapped wave would have decayed 99.5 percent before reaching this current meter and could not be observed. The maximum trapping frequency at this mooring never exceeded $\omega_c = 2.0$ cpd and no semidiurnal trapping occurred.
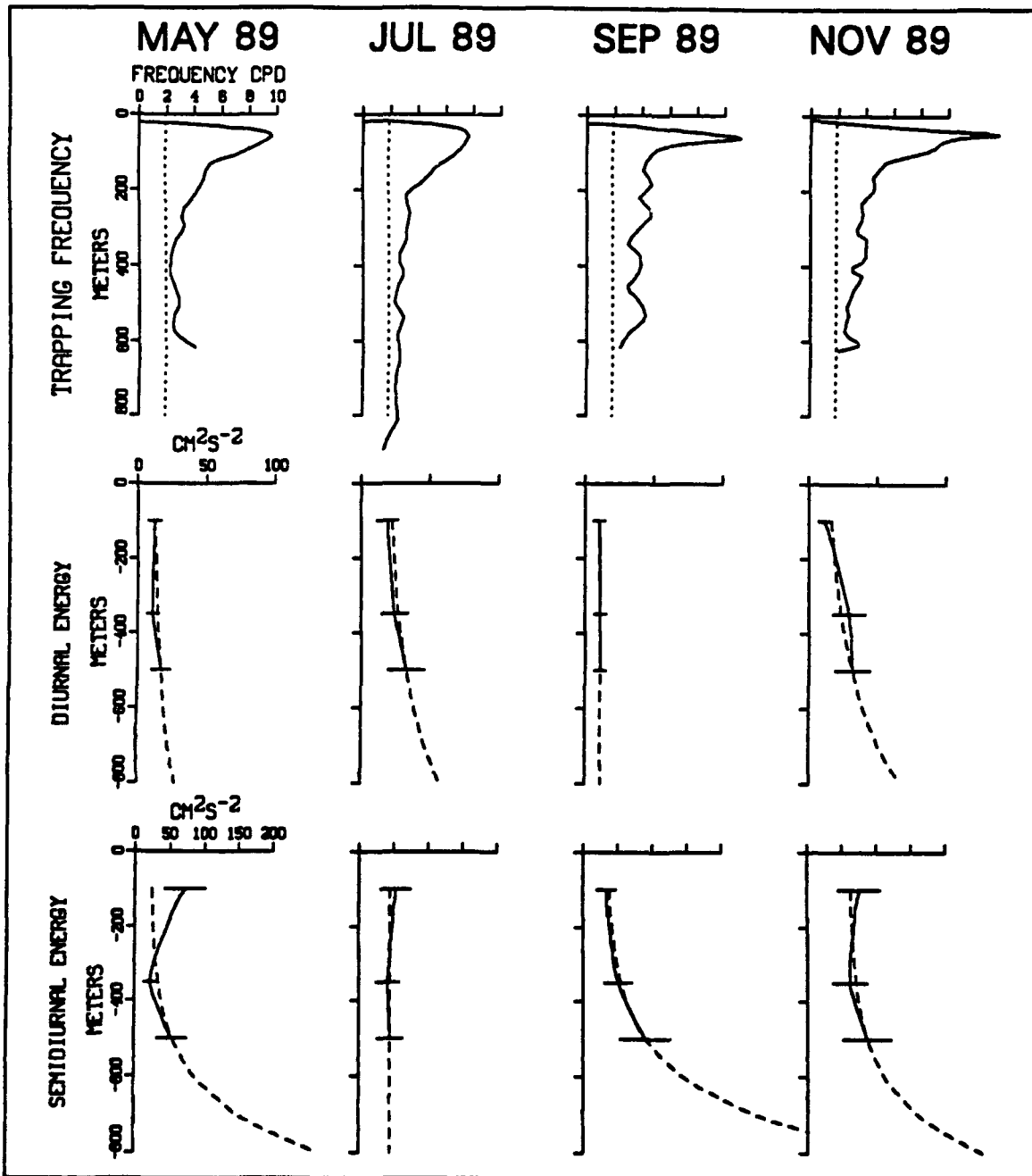
Figure 23.   Trapping Frequencies and Energy Profiles at P2 During 1989:   Maximum trapping frequencies are plotted against depth with the dashed line indicating 2.0 cpd in the top row. The middle row shows observed diurnal spectral energy profiles (solid lines) with 95% confidence intervals (horizontal bars). Theoretical energy profiles (dashed lines), based on a decay scale calculated using N from the bottom of CTD casts (or at 800 m for July 1989) , are matched to the observations at 500 m. Similar profiles are shown in the third row for semidiurnal energy.
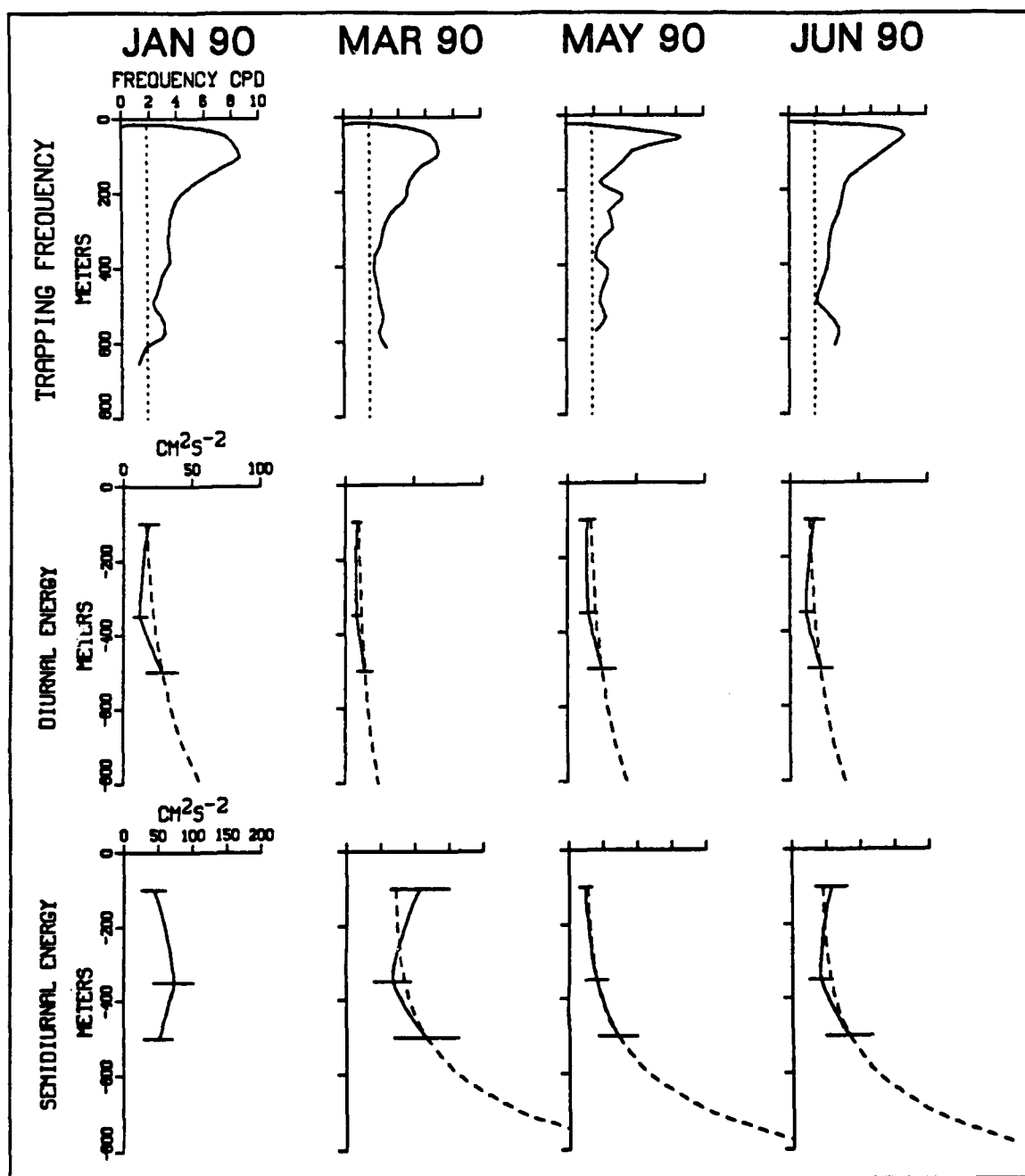
Figure 24. Trapping Frequencies and Energy Profiles at P2 During 1990: Data is plotted as described in Figure 23. No theoretical semidiurnal energy profile is shown for January 1990 when $N \sin \alpha$ near the bottom was less than 2.0 cpd.

V. DISCUSSION

A. BOTTOM TRAPPED WAVES

The trapping or amplification of tidal band kinetic energy near the ocean bottom was evident from the data obtained at mooring P2. Both the current ellipses and the energy distribution displayed a significant increase from a depth of 350 m to 500 m during the seventeen months of data analyzed. A similar increase was not evident from the data obtained at mooring P3.

The two methods of analysis used to examine the currents produced results which were in general agreement. The energy levels derived through complex demodulation and current ellipses were larger in magnitude than those obtained through spectral analysis. The total KE represented by the ellipses was 10.7 % greater than the energy obtained from spectral analysis. The lower energy spectral analysis values may be due to Doppler shifting of small wavelength internal tides to other parts of the spectrum. This shifting could spread energy around the tidal band so that energy measured precisely at the frequency of a tide, using the high resolution FFT of VCSPC3, improperly excluded tidal energy located in sidebands (*Wunsh*, 1975). The difference between the energy from ellipses and spectral analysis was greatest at P3 during December 1989. The spectral density plots for the current meter records at 100 m and 350 m show that the diurnal peak was spread out over a wider frequency band (perhaps by Doppler shifting) and had a smaller amplitude than for other months of the same record.

Both ellipses and spectral energy profiles indicated more energy was present at 100 m than at 350 m at both moorings for diurnal and semidiurnal currents. The current meters at 100 m were above the main pycnocline and the higher energy levels in the surface layer could be the result of wind forcing at or near tidal frequencies. Strong

coastal winds with diurnal variations have often been observed along the California coast (*Beardsley et al.*, 1987). The pycnocline could prevent coupling of surface energy to deeper layers. Diurnal tidal currents may also be influenced by inertial currents with a frequency is 1.1 cpd off Point Sur. The narrow frequency separation between diurnal and inertial currents could result in smearing or leakage of energy into the diurnal band.

The observed distribution of tidal energy had a vertical decay rate indicative of bottom trapping at mooring P2. The fit of a theoretical curve to the data fell within the 95 percent confidence intervals with few exceptions. In January 1990 the observed diurnal energy at 350 m was less than predicted by bottom trapped theory using the buoyancy frequency calculated from a single CTD cast. If the buoyancy frequency had been greater the trapping coefficient, κ, would have been larger. A larger κ would result in a faster decay rate and the theoretical energy at 350 m would have been closer to observations. The semidiurnal energy at 100 m during May 1989 was higher than expected using the modeled decay curve and these energetic semidiurnal currents may result from surface (wind) forcing. Another factor in the vertical semidiurnal energy distribution is free internal waves which exist at superinertial frequencies. Free internal waves could be generated by tidal forcing across the continental shelf break and could then propagate into deeper stratified water (*Baines*, 1982). Horizontal velocities over the shelf have been observed where the highest velocities were near the surface and bottom. The velocity structure was attributed to the first dynamical mode (*Rosenfeld*, 1990) and the same structure may dominate internal tides over the continental slope. The semidiurnal currents at P2, located close to the shelf break, were twice as energetic as the semidiurnal currents found further offshore at P3 and did have more energy at the top and bottom current meters (100 m and 500 m) than at the middle (350 m). Bottom trapping did not occur with any discernable seasonal pattern. The absence of distinct

51

temporal variation agrees with other observations of internal tides along the California coast (*Noble et al.*, 1987).

The theoretical curves plotted for P2 in Figures 23 and 24 were extrapolated to 800 m. The average diurnal energy represented by these estimates was 40.5 cm^2 sec^{-2}. Using the average diurnal current ellipse eccentricity ($e = 3.42$), diurnal currents at 800 m would have had a semi-major axis of 6.1 cm sec^{-1} and a semi-minor axis of 1.8 cm sec^{-1}. The theoretical energy for semidiurnal currents extrapolated to 800 m was 310.0 cm^2 sec^{-2}. An average semidiurnal eccentricity of $e = 3.26$ produced an ellipse representing bottom currents with semi-major and semi-minor axis lengths of 16.8 cm sec^{-1} and 5.2 cm sec^{-1} respectively. The magnitude of these currents is reasonable, however, bottom trapped theory assumes inviscid boundary conditions and bottom friction may reduce the velocity of predicted bottom trapped currents.

The average wavelength of bottom trapped diurnal waves, computed using the average trapping coefficient in Table 5, was 66.5 km. The average wavelength of bottom trapped semidiurnal waves was 33.2 km. This compares favorably to first baroclinic mode internal waves of semidiurnal frequency observed during CODE which had wavelengths between 20 and 30 km (*Rosenfeld*, 1990).

The rotation of tidal current ellipses is not described by bottom trapped theory. The observed rotation of the current ellipses was variable with 73 percent of the diurnal ellipses rotating counterclockwise and 52 percent of the semidiurnal ellipses rotating clockwise. Barotropic Kelvin waves, free internal waves and shelf waves all influence the rotation of current ellipses at tidal frequencies. The observed direction of rotation is determined by the cumulative effect of these unresolved wave regimes.

Barotropic semidiurnal tides are dominated by the M_2 constituent. The horizontal velocities generated by Kelvin waves at this frequency are normally aligned with topography (*Noble et al.*, 1987). The observed tidal current ellipses all had cross-slope com-

ponents and vertical velocity structures which may reflect the influence of a baroclinic wave structure. At the deepest current meters, the diurnal current ellipses were oriented more across the bottom slope ($P2 = 44°$, $P3 = 54°$) than were the semidiurnal ellipses ($P2 = 25°$, $P3 = 23°$). With this geometry the particle motion of diurnal currents had a larger upslope component and more bottom trapping than semidiurnal currents of the same magnitude. Even though observed diurnal currents were significantly less energetic than semidiurnal currents, diurnal bottom trapping was always evident at mooring P2.

Both moorings had a similar bottom slope α and the currents analyzed were limited to diurnal and semidiurnal frequencies. The only variable in determining the limiting trapping frequency ($\omega_c = N \sin \alpha$) was the buoyancy frequency. Higher values of N resulted in higher trapping frequencies. For each of the eight months when CTD casts were made at P2, diurnal trapping was possible as indicated by the calculated values of ω_c and semidiurnal trapping was indicated during seven of these months. The current ellipses and energy profiles exhibited bottom trapping in each case. No bottom trapping was evident at P3 although there were two months with ω_c values high enough to permit the trapping of diurnal energy. The absence of any notable bottom trapping at P3 may be due to the trapping scale and the depth of the instruments at that mooring. All three current meters at P3 were above the e-folding depths of bottom trapped diurnal and semidiurnal energy. If any trapped energy was present, the magnitude of the signal was indiscernible at the P3 current meters.

The difference in maximum trapping frequencies at each mooring is caused by different hydrographic conditions at P2 and P3. The cruise of November 1989 can be used to illustrate typical conditions. Density gradients are greater near the ocean bottom at P2 than at P3 (Figure 25) and the gradients produce higher N values at P2 than those calculated at P3. The stronger gradients at P2 permit trapping of waves with frequencies higher than the maximum frequency of trapped waves at mooring P3.

STNOV89
SIGMA T

7 6 5 4 3 2 1

10 KM

Pressure (db)

25.5 25.5 26.0 25.5
26.3 26.3
26.5
26.6 26.6 26.6
26.7
26.8 26.8 26.8
26.9
27.0 27.0 27.0
27.1
27.2 27.2
27.3 27.3
27.4 27.4
27.5
27.6

P2

P3
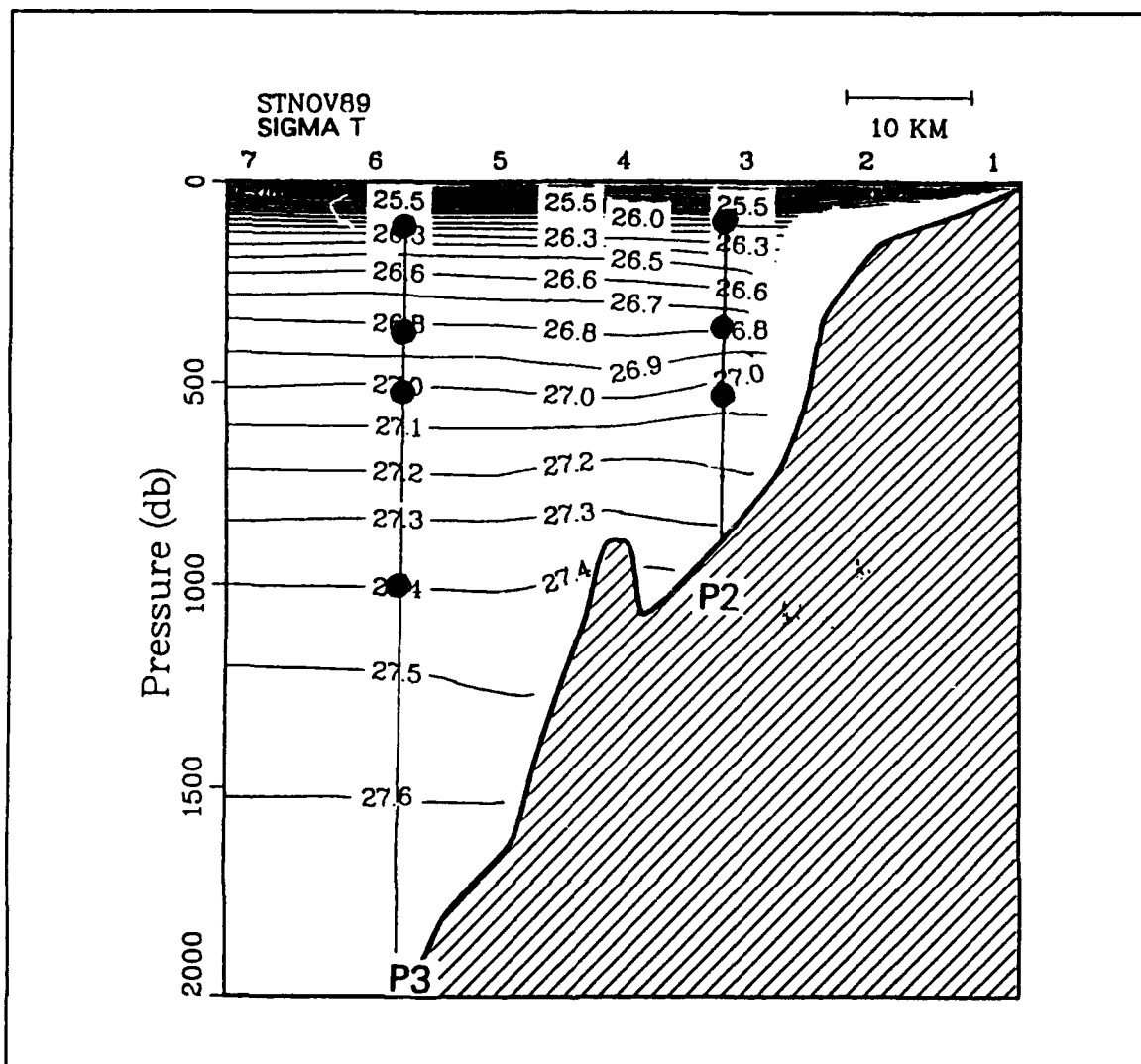
Figure 25. Vertical Density Section Off Point Sur, California During November, 1989: The positions of moorings P2 and P3 are indicated.

B. LIMITATIONS

Several assumptions were made in comparing the observations at P2 with theoretical predictions for bottom trapped waves. The first was that the tidal currents were always oriented across the sea floor slope so that the angle $\phi = 90°$. This angle permits maximum trapping and simplifies the equation $\sigma = N \sin \alpha \sin \phi$ to $\omega_c = N \sin \alpha$. At angles less than 90°, the limiting trapping frequency ω_c will be lower and the bottom trapping of tidal energy may not occur. If ϕ was assumed to be the angle at which the semi-major

axis of the tidal current ellipses crossed the bottom contours, then the maximum trapping frequency σ at P2 ($\phi = 44°$ at 500 m) would still exceed 1.0 cpd for seven of the eight months when N values were available. For the P2 semidiurnal ellipses ($\phi = 25°$ at 500 m), σ would not have exceeded 2.0 cpd for any month. If no semidiurnal trapping was possible, then the vertical distribution of energy at semidiurnal frequencies must be attributed to other factors including free internal waves.

A second assumption was that a single CTD cast provided information which could be used to interpret monthly averaged current meter data. The CTD casts typically ended 50 m above the sea floor and salinity and temperature values over the deepest 10 m interval were used to calculate N for each month. These N values were assumed to be constant from the bottom of the CTD cast to the sea floor. Trapping frequencies calculated with N were similarly extrapolated. The use of extrapolated values was supported by the CTD cast of July 1989 which was slightly offshore of mooring P2 and extended to 903 m (the 10 m interval centered at 800 m was used to calculate N at P2). The values of N were fairly constant during July 1989 (42.2 cpd - 40.9cpd) at the depths where extrapolation was used (650 m to 800 m) for the seven other CTD casts. As discussed in the previous section, variations in N could affect the fit of the theoretical decay curves to observations. The ω_c and κ values using a constant N were compared to ω_c and κ computed using N obtained by extending the slope of the N^2 curves to 800 m. The differences created slight variations of ω_c which did not conflict with any of the results presented in Chapter IV. The differences in the κ values were very small and considered insignificant.

The instrumentation at each of the moorings was not ideally positioned for the study of bottom trapped waves. The current meters were too sparse to provide a good profile of the currents throughout the water column. The current meters at the 100 m level were above the pycnocline and may have contained energy from surface forcing which was

not considered in constructing the theoretical decay curves. The lowest current meters at P2 and P3 were not deep enough to detect the strongest currents expected near the bottom. At P3 the small trapping scales made it unlikely that any signal from a bottom trapped wave could be detected. The current meter at 1000 m was well above the e-folding depth of diurnal and semidiurnal waves. Additionally, the location of P3 in an area with relatively weak density gradients restricted most bottom trapping to subtidal frequencies.

VI. CONCLUSIONS AND RECOMMENDATIONS

The analysis of current meter records from moorings located off Point Sur, California showed an increase of energy at tidal frequencies with depth. This can potentially be explained using the theory of Rhines (1970) for bottom trapped waves over the continental slope. The increased energy was observed whenever bottom slope, water stratification and frequency met prescribed conditions.

Seventeen months of current meter data was examined from mooring P2. The data were examined using complex demodulation and spectral analysis. At mooring P2, bottom trapped energy at the diurnal frequency was observed for each month analyzed. Bottom trapping occurred at semidiurnal frequencies for fourteen of the seventeen months but the energy contribution due to free internal waves, which influenced the semidiurnal results, was not determined. Bottom trapping at mooring P2 occurred during each month of the year and no seasonal patterns could be distinguished. The maximum trapping frequency at P2, computed using $N \sin \alpha$, was an accurate indicator of bottom trapping at tidal frequencies.

No bottom trapping was observed at mooring P3 using data collected over six months. Weak density gradients near the sea floor often kept the maximum trapped frequency below the tidal frequencies. The current meters at this mooring were positioned too far above the sea floor for detection of bottom trapped waves at diurnal or semidiurnal frequencies.

The bottom trapped wave theory described by Rhines (1970) was also used to calculate vertical decay scales and energy distribution profiles. The theoretical decay was modeled using hydrographic data collected near the mooring locations. In most cases

57

the modeled decay agreed with the observed decay of tidal energy away from the sea floor within the error of the calculation.

The tidal currents off Point Sur are the most energetic currents found over the continental slope. The semidiurnal currents dominate but diurnal currents can be significant, particularly when amplification due to bottom trapping occurs. Further study of bottom trapping should be conducted using the continuing current meter arrays at or near the location of P2. Additional deep instrumentation, particularly just above the sea floor, is needed to adequately study this phenomena. Because trapping was observed throughout the year, a short deployment of a few months length may collect sufficient data to verify trapping at tidal frequencies. Tidal currents are at the upper limit of the range of trapped waves and longer deployments could be used to examine coastally trapped waves occurring at much lower frequencies under the same conditions.

REFERENCES

Aanderaa Instruments Technical Description No. 159, 1990: *Operating Manual RCM 7 & 8*, Aanderaa Instruments, Bergen, Norway, 74 pp.

Baines, P. G., 1982: "On Internal Tide Generation Models", *Deep Sea Res.*, 29, 307-338.

Beardsley, R. C., C. E. Dorman, C. A. Friehe, L. K. Rosenfeld, and C. D. Winant, 1987: "Local Atmospheric Forcing During the Coastal Ocean Dynamics Experiment 1. A Description of the Marine Boundary Layer and Atmospheric Conditions Over a Northern California Upwelling Region", *J. Geophys. Res.*, 92,, 1467-1488.

Bendat, J. S., and A. G. Piersol, 1986: *Random Data Analysis and Measurement Procedures*, John Wiley and Sons, Inc., New York, New York, 586 pp.

Denbo, D. W., K. Lolain, J. S. Allen, A. Huyer and R. L. Smith, 1984: "Current Meter Observations over the Continental Shelf Off Oregon and California February 1981 - January 1984", Data Report 112, Ref. 84-12, November 1984, College of Oceanography, Oregon State University, Corvallis, Oregon.

Dronkers, J. J., 1964: *Tidal Computations in Rivers and Coastal Waters*, North-Holland Publishing Co., Amsterdam, 306 pp.

Gerald, C. F. and P. O. Wheatly, 1989: *Applied Numerical Analysis*, Addison-Wesley Publishing Co., New York, New York, 679 pp.

Millero, F. J. and A. Poisson, 1981: "International One-Atmosphere Equation of State for Seawater", *Deep-Sea Research*, 28A, 625-629.

Munk, W., F. Snodgrass and M. Wimbush, 1970: "Tides Off-Shore: Transition from California Coastal to Deep-Sea Waters", *J. Geophys. Fluid Dynamics*, 1, 161-235.

Noble, M., L. K. Rosenfeld, R. L. Smith, J. V. Gardner, and R. C. Beardsley, 1987: "Tidal Currents Seaward of the Northern California Continental Shelf", *J. Geophys. Res.*, 92, 1733-1744.

Pugh, D. T., 1986: *Tides, Surges and Mean Sea Level*, John Wiley & Sons Ltd., Chichester, Great Britain, 472 pp.

Rhines, P., 1970: "Edge-, Bottom-, and Rossby Waves in a Rotating Stratified Fluid", *J. Geophys. Fluid Dynamics*, 1, 273-302.

Rosenfeld, L. K., 1990: "Baroclinic Semidiurnal Tidal Currents Over the Continental Shelf off Northern California:, *J. Geophy. Res.*, 95, 22153-22,172.

Schureman, P., 1958: *Manual of Harmonic Analysis and Prediction of Tides*, United States Government Printing Office, Washington D.C., 317 pp.

Thompson, R. O. R. Y., and J. R. Luyten, 1976: "Evidence for Bottom-trapped Topographic Rossby Waves from Single Moorings", *Deep-Sea Research*, **23**, 629-635.

Tisch, T. D., 1990: *Seasonal Variability of the Geostrophic Velocity and Water Mass Structure off Point Sur, California.* Master's Thesis, Naval Postgraduate School, Monterey, California, 163 pp.

Wunsh, C., 1975: "Internal Tides in the Ocean", *Rev. Geophys.*, **18**, 167-182.

INITIAL DISTRIBUTION LIST

		No. Copies
1.	Defense Technical Information Center Cameron Station Alexandria, VA 22304-6145	2
2.	Library, Code 52 Naval Postgraduate School Monterey, CA 93943-5002	2
3.	Chairman (Code OC/Co) Department of Oceanography Naval Postgraduate School Monterey, CA 93943-5000	1
4.	Chairman (Code MR/Hy) Department of Meteorology Naval Postgraduate School Monterey, CA 93943-5000	1
5.	Dr. S. R. Ramp (Code OC/Ra) Department of Oceanography Naval Postgraduate School Monterey, CA 93943-5000	1
6.	Dr. L. K. Rosenfeld (Code OC/Ro) Department of Oceanography Naval Postgraduate School Monterey, CA 93943-5000	1
7.	LCDR S. L. Sielbeck, USCG Commanding Officer USCGC MALLOW (WLB 396) FPO San Francisco, CA 96672-3913	1
8.	Commandant (G-PO-2) U.S. Coast Guard Washington, D.C. 20593	2
9.	Dr. R. C. Beardsley Dept. of Physical Oceanography Clark Laboratory, Woods Hole Oceanographic Institution Woods Hole, MA 02543	1
10.	Dr. M. Noble U.S. Geological Survey 345 Middlefield Road, MS 999 Menlo Park, CA 94025	1

61

11. Dr. T. Kinder   1
    Office of Naval Research, Code 1122CS
    800 N. Quincy Street
    Arlington, VA 22217

12. Superintendent (ds)   1
    U.S. Coast Guard Academy
    15 Mohegan Avenue
    New London, CT 06320-4195